Regulation of meiotic progression by Sertoli-cell androgen signaling

Hailey Larose[a,†], Travis Kent[b,†], Qianyi Ma[a,c], Adrienne Niederriter Shami[a], Nadia Harerimana[d], Jun Z. Li[a,c], Saher Sue Hammoud[a,e,f,*], and Mary Ann Handel[b,*]

[a]Department of Human Genetics, [c]Department of Computational Medicine and Bioinformatics, [e]Department of Obstetrics and Gynecology, [f]Department of Urology, University of Michigan, Ann Arbor, MI 48109; [b]The Jackson Laboratory, Bar Harbor, ME 04609; [d]College of the Atlantic, Bar Harbor ME 04609

ABSTRACT **Androgen receptor (AR) signaling in Sertoli cells is known to be important for germ-cell progression through meiosis, but the extent to which androgens indirectly regulate specific meiotic stages is not known. Here, we combine synchronization of spermatogenesis, cytological analyses and single-cell RNAseq (scRNAseq) in the Sertoli-cell androgen receptor knockout (SCARKO) mutant and control mice, and demonstrate that SCARKO mutant spermatocytes exhibited normal expression and localization of key protein markers of meiotic prophase events, indicating that initiation of meiotic prophase is not androgen dependent. However, spermatocytes from SCARKO testes failed to acquire competence for the meiotic division phase. ScRNAseq analysis of wild-type and SCARKO mutant testes revealed a molecular transcriptomic block in an early meiotic prophase state (leptotene/zygotene) in mutant germ cells, and identified several misregulated genes in SCARKO Sertoli cells, many of which have been previously implicated in male infertility. Together, our coordinated cytological and scRNAseq analyses identified germ-cell intrinsic and extrinsic genes responsive to Sertoli-cell androgen signaling that promotes cellular states permissive for the meiotic division phase.**

Monitoring Editor
Julie Brill
The Hospital for Sick Children

Received: May 26, 2020
Revised: Sep 22, 2020
Accepted: Sep 29, 2020

INTRODUCTION

Mammalian germ cells receive direct and indirect signaling from testicular somatic cells that provide the environment, and in some cases, instructive cues, for germ cell development and differentiation. Within the seminiferous tubules, Sertoli cells are the only niche cells that are in direct contact with germ cell populations, thus supporting all stages of their development, including meiosis, which ultimately leads to production of haploid gametes (Griswold, 2016; Bolcun-Filas and Handel, 2018; Kent *et al.*, 2019). Previous studies have shown that androgens, and specifically androgen receptor (AR) signaling in Sertoli cells, is one mechanism by which meiotic progress is regulated (de Gendt *et al.*, 2004), but exactly how AR signaling in neighboring Sertoli cells promotes the events of meiosis is not well understood.

During the substages of the first meiotic prophase (leptonema, zygonema, pachynema and diplonema), homologous chromosomes line up to form diploid pairs (synapsis), and undergo recombination. At the end of meiotic prophase, spermatocytes rapidly undergo the first reductive division, which segregates the homologues from each other, followed by the second equational division, which separates sister chromatids to generate 4 haploid gametes (described in detail in Bolcun-Filas and Handel, 2018). Multiple kinases have been implicated to regulate the onset of the first meiotic division, termed the G2-MI transition, but the mechanism by which it is initiated have been difficult to delineate (Sun and Handel, 2008; Jordan *et al.*, 2012). However, we know that spermatocytes acquire competency for the G2-MI transition several days before division occurs. This was revealed in early work (Cobb *et al.*, 1999) in which okadaic acid (OA), a pleitropic phosphatase inhibitor used in a variety of systems to prompt cell division-related condensation of chromosomes, was found to trigger precocious induction of the G2-MI

This article was published online ahead of print in MBoC in Press (http://www.molbiolcell.org/cgi/doi/10.1091/mbc.E20-05-0334) on October 7, 2020.

†These individuals contributed equally to the work.

*Address correspondence to: Saher Sue Hammoud (hammou@umich.edu); Mary Ann Handel (maryann.handel@jax.org).

Abbreviations used: AR, androgen receptor; BSA, bovine serum albumin; CCA, canonical correlation analysis; DE, differential expression; dpi, days postinjection; dpp, days postpartum; DSB, double-strand break; FBS, fetal bovine serum; KO, knockout; OA, okadaic acid; PBS, phosphate-buffered saline; SC, synaptonemal complex; scRNAseq, single-cell RNAseq; SCARKO, Sertoli cell androgen receptor knockout; WT, wild type.

transition in male germ cells. Competency to undergo this response to OA is acquired concomitently with the appearance of the H1t histone variant, formally known as H1F6 (Cobb *et al.*, 1999), but the H1t histone variant is not required for germ cells to enter the meiotic division phase (Lin *et al.*, 2000).

Progress of meiotic prophase and acquisition of meiotic competence are typically perceived as germ cell-intrinsic processes, but emerging molecular profiling studies suggest that neighboring testicular somatic cells, and in particular Sertoli cells, may directly or indirectly control these meiotic events. Interestingly, Sertoli cells undergo distinct molecular and metabolic changes across the seminiferous tubule. In adult mammals, the seminiferous epithelium regularly cycles through distinct stages, each one of which is morphologically defined by recurring germ cell states (e.g., characteristic associations of spermatogonial populations, meiotic prophase cells, round/elongating spermatids, etc.), as well as distinct molecular and metabolic Sertoli cell states (Chen *et al.*, 2018; Green *et al.*, 2018). These histological associations define the stages (12 in mice) of the seminiferous epithelium cycle, setting both the environment and the pace within which germ cell differentiation unfolds (Kent *et al.*, 2019).

One required and dynamically regulated signaling pathway across the seminiferous epithelial stages is androgen signaling. Genetic loss-of-function experiments show that global knockout (KO) of the *Ar* gene abrogates testis development and spermatogenesis (O'Hara and Smith, 2015), although the germ cells themselves do not require cell-autonomous expression of ARs (Johnston *et al.*, 2001). AR is expressed by many somatic cell types in the testis, but AR transcript and protein levels in Sertoli cells peak at Stages VI-VII, coincident with differentiating spermatogonia committing to meiotic prophase entry (O'Hara and Smith, 2015), suggesting that Sertoli-cell AR signaling may mediate stage-specific roles in meiosis. Indeed, in a conditional Sertoli-cell only Ar knockout, referred to as the SCARKO mouse model, spermatogenesis is arrested in meiosis (De Gendt *et al.*, 2004), but there are some differences among reports as to which specific events of meiosis are affected (Chen *et al.*, 2016).

In our work, we asked if androgen signaling is required for acquisition of competence for meiotic division and, if so, how androgen shapes the transcriptional landscape of spermatocytes to instruct progress through meiotic prophase. Because asynchronous and iterative waves of spermatogenesis across the seminiferous epithelium generate multiple germ cell stages within a given cross-section of the testis, it has previously been difficult to parse out interactions among major events of meiosis and their stage specificity. However, now methods are available to manipulate availability of retinoic acid (RA) in the mouse testis, thus precisely synchronizing the onset of spermatogenesis so that only one to three temporally adjacent stages are represented at any moment (Hogarth *et al.*, 2013, 2015; Griswold, 2016). Thus, it is possible to apply this methodology to relate seminiferous epithelium stage-specific Sertoli cell signaling events to the spermatogenic, and more specifically, meiotic, events they control. Using stage-synchronized testes samples (Figure 1; Supplemental Table S1) from the SCARKO mice, we investigated the cytological hallmarks of meiotic prophase and the temporal acquisition of division-phase competence. We also performed parallel single-cell transcriptomic (scRNAseq) analyses to determine androgen-regulated transcriptional markers of meiotic progress.

We confirmed that Sertoli-cell AR signaling is required for the overall survival of meiotic prophase spermatocytes, while in the absence of AR, germ cells are progressively lost. Among surviving spermatocytes that enter meiotic prophase in SCARKO mouse testes, chromosome synapsis and recombination occurred normally,

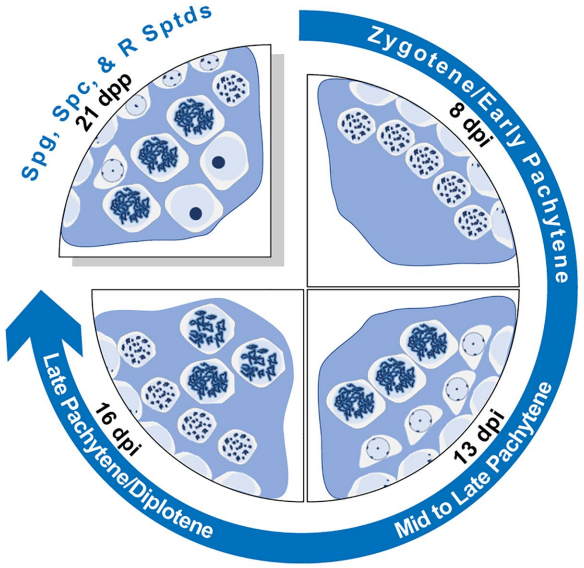

FIGURE 1: Experimental strategy and source of cells for scRNAseq. In this schematic of seminiferous tubule cross-sections, the first three quadrants, with the blue arrow, illustrate the cell populations retrieved at 8, 13, and 16 dpi of RA to synchronize spermatogenesis. The fourth quadrant illustrates the germ-cell composition of seminiferous tubules retrieved at 21 d of age (21 dpp), with no manipulation of RA. The cell populations include spermatogonia (Spg), spermatocytes (Spc) in various substages of meiotic prophase, and spermatids (Sptd).

suggesting that early meiotic prophase events are not dependent on Sertoli-cell AR signaling. However, we discovered that Sertoli-cell AR signaling is required for spermatocytes to acquire competence to enter the meiotic division phase, explaining the observed cytological arrest in spermatocytes of SCARKO testes. To achieve a comprehensive and unbiased molecular understanding of the SCARKO phenotype, we leveraged our testicular germ cell synchronization (Figure 1; Supplemental Table S1) and single-cell transcriptomics analysis, which enabled us to pinpoint a set of spermatocyte-expressed genes regulated by AR signaling in a noncell-autonomous manner. Many of the genes have likely or known postmeiotic roles, suggesting that this gene set may function to license spermatocytes for progression toward spermiogenesis. Overall, these findings reveal the molecular machinery by which androgen signaling in Sertoli cells creates a permissive environment for germ-cell progression through meiosis and gamete production.

RESULTS

Sertoli cell-expressed AR is functionally required to maintain germ cell numbers

Consistent with previous reports on additional SCARKO models (De Gendt *et al.*, 2004); (Chang *et al.*, 2004), our histological analyses of testes from 21 d postpartum (dpp) SCARKO males (Supplemental Table S1) revealed both loss of meiotic germ cells and failure of surviving spermatocytes to progress. Most spermatocytes appeared arrested at early to midmeiotic prophase I, with very few completing the first meiotic division (Figure 2A). To assess the extent of apoptosis, we synchronized seminiferous tubules in experimental animals and conducted TUNEL analysis on wild-type (WT) and synchronized SCARKO testes collected at 8, 10, 12, 14, and 16 d post-RA injection (dpi) (Figure 2B; Supplemental Table S1). As expected, histological testis sections from WT animals were enriched for germ cells at late leptotene/early zygotene (8 dpi), late zygotene/early pachytene

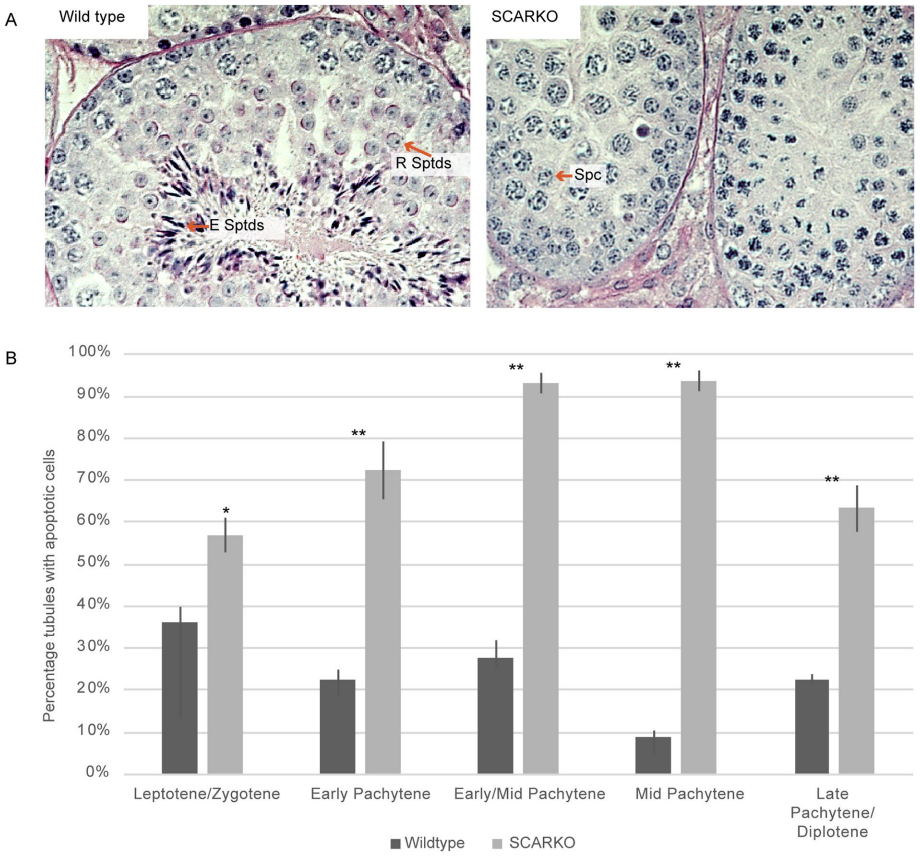

FIGURE 2: SCARKO testes exhibit germ-cell arrest and progressive loss. (A) Cross-sections of WT (L) and SCARKO (R) adult testes. The WT germ cells develop to spermatids (R Sptds) and elongated spermatids (E Sptds), whereas most germ cells in SCARKO testes develop only to spermatocytes (Spc). (B) Percentage of tubules with TUNEL-positive cells from testes of both WT and SCARKO males at 8, 10, 12, 14, and 16 dpi.

(10 dpi), early–midpachytene (12 dpi), mid/late pachytene (14 dpi), and late pachynema/diplotene (16 dpi) stages (Supplemental Table S1). However, the percentage of apoptotic cells per tubule in SCARKO testes was significantly increased at all stages except preleptonema (Figure 2B). These histological observations are consistent with both progressive germ-cell loss due to apoptosis and failure to differentiate beyond meiotic prophase in the absence of androgen signaling from Sertoli cells.

Spermatocytes in SCARKO mice enter prophase, but fail to acquire competence for initating meiotic division

Given the almost complete absence of postmeiotic germ cells in SCARKO testes, we determined whether classical protein markers for meiotic prophase milestones were expressed in spermatocytes. We assessed markers for chromosome pairing and synapsis, proteins involved in meiotic homologous recombination, and the differentiation marker (histone H1t), whose expression coincides with onset of pachytene and acquisition of competence for meiotic division (Inselman *et al.*, 2003, Cobb *et al.*, 1999). To assess homologous chromosome pairing and the synaptonemal complex (SC) integrity, we used antibodies recognizing the SC-associated proteins SYCP3 and SYCP1 (marking the lateral and central element established at synapsis, respectively). Spermatocytes from both WT and SCARKO testes appeared to be capable of assembling normal SCs, as indicated by labeling for SYCP3 and SYCP1 (Figure 3, A and C). In early stages of meiotic prophase, phosphorylated histone H2AX (γH2AX) is dispersed throughout the chromatin, indicating formation of recombination-related double-strand breaks (DSBs). In the pachytene stage, γH2AX becomes restricted to the XY body, indicating that most DSBs have been repaired. When examining this progression in synchronized and nonsynchronized WT and SCARKO spermatocytes, we found that γH2AX staining patterns were generally similar, although some abnormalities were observed in spermatocytes from SCARKO mutants (Figure 3, A and B). Similarly, MLH1 distribution, which corresponds to the number and distribution of chiasmata, was comparable in WT and SCARKO spermatocytes (Figure 3D). Finally, we assessed whether the germ cells progress through pachynema by staining for histone H1t (Inselman *et al.*, 2003). Because germ cells in SCARKO testes gradually become depleted due to apoptosis, we analyzed germ cells at the same developmental stages from synchronized WT and SCARKO testes and found no differences in the number of H1t-positive spermatocytes (Figure 3, E and F). This observation indicates that midpachytene expression and localization of H1t on chromsome is not regulated by Sertoli-cell AR signaling. Taken together, our analysis of meiotic prophase markers suggests that loss of AR in Sertoli cells does not impede chromosome synapsis, recombination events, or accumulation of histone H1t in spermatocytes that escape apoptosis.

These observations raise a fundamental question: Why do germ cells that progress to mid- to late meiotic prophase in SCARKO testes fail to undergo meiotic division? To answer this question, we treated spermatocytes with the phosphatase inhibitor, OA, a regime that induces chromosome condensation and entry into metaphase by meiotically competent spermatocytes (Cobb *et al.*, 1999). Testes were isolated at 14, 15, and 16 dpi, when spermatocytes correspond to those in seminiferous epithelial stages VII-VIII, VIII-IX, and X-XI, respectively, which are enriched for spermatocytes at mid- to late pachynema. As expected, OA treatment resulted in spermatocytes in a pachytene configuration, or, from metaphase-competent spermatocytes, with condensed metaphase bivalents (Figure 3G). We did not observe any OA-induced condensation of meiotic bivalents at 14 dpi in spermatocytes from either SCARKO or WT testes (Figure 3H). At 15 and 16 dpi, only 5–25% of pachytene spermatocytes from synchronized SCARKO mutant mice were competent to condense chromosomes and enter metaphase, compared with ~90–95% from WT mice (Figure 3H). This analysis reveals that although SCARKO spermatocytes are at a comparable cytological state as WT cells, they have not acquired the inherent competence to respond to OA. This functional difference may stem from AR signaling-dependent molecular circuitry governing acquisition of competency.

scRNAseq reveals early meiotic arrest of spermatocytes in SCARKO mutants

We next set out to investigate how the absence of AR signaling from Sertoli cells impacts the germ cell transcriptional landscape and the

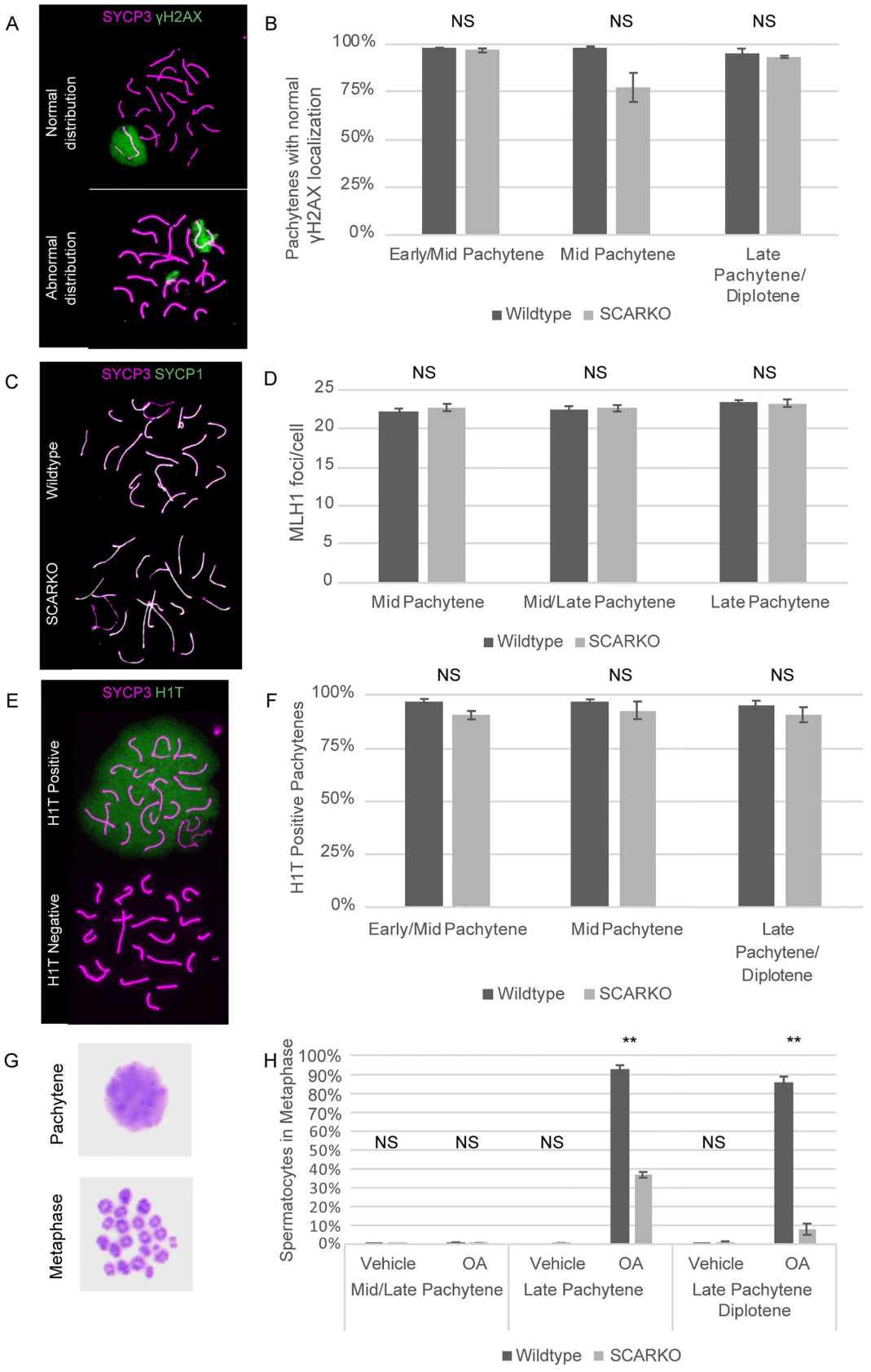

FIGURE 3: Many features of meiosis are normal in SCARKO testes, but spermatocytes do not acquire competence for the OA-induced meiotic division phase. (A) At the pachytene substage of meiotic prophase, SCARKO spermatocytes, labeled with anti-SYCP3 to identify chromosomal axes, exhibit both normal distribution of γH2AX, restricted to the XY body, and abnormal patterns with γH2AX also in the autosomal domain. (B) Distribution of γH2AX scored in pachytene spermatocytes isolated from WT and SCARKO synchronized testes, with the *x*-axis indicating the stages of pachytene

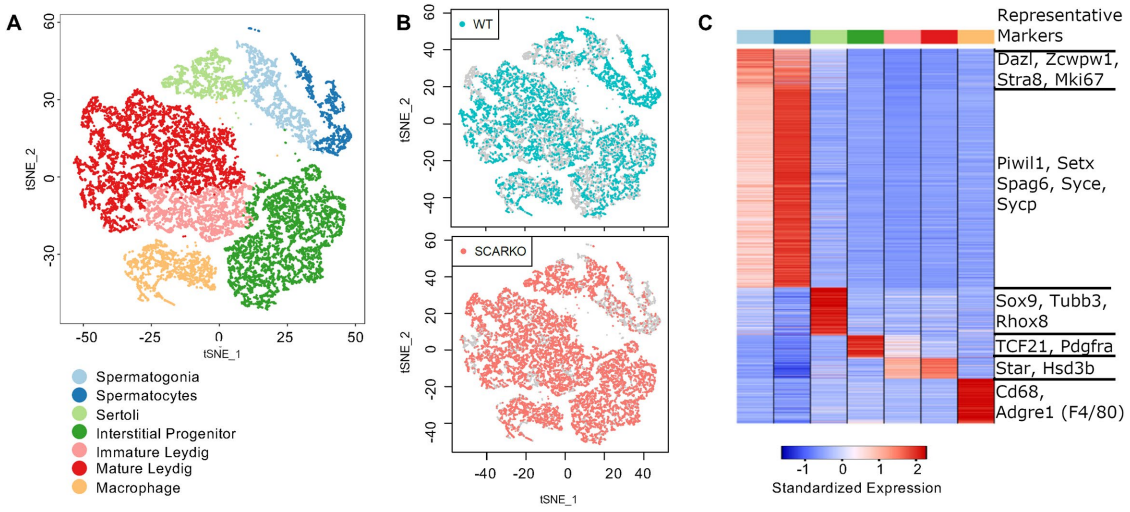

FIGURE 4: Overview of major cell types and cellular attributes inferred from single-cell RNA-Seq analyses of WT and SCARKO mouse testes. **(A)** Global heterogeneity among the ~21,000 cells for both genotypes over all time-points of collection, shown in tSNE plot and colored by the 7 clusters discovered, corresponding to two germ cell populations and five somatic cell types. The cell populations include spermatogonia (Spg), spermatocytes (Spc) in various substages of meiotic prophase, Sertoli, interstitial progenitor, immature Leydig, Mature Leydig, and Macrophages. **(B)** Same visualization as in A, but colored by WT and SCARKO separately, showing that cells from the two genotypes are matched in number, and occupy comparable tSNE space, except for fewer spermatogonia and spermatocytes in SCARKO. (C) Marker genes for the 7 cell types, shown as a heatmap where each marker's values have been standardized over the cluster centroids. Cell types are indicated on top, following the same color scheme as in A. Indicated on the right are representative genes, some of which are also shown in Supplemental Supplemental Figure S2.

ultimate ability of germ cells to acquire meiotic competence.To this end, we performed scRNAseq on whole testis cell suspensions from 21 dpp WT and SCARKO males, an age in which all germ cell stages of interest are present (Figure 1; Supplemental Table S1) and from synchronized testes to enrich for germ cells at particular stages of meiotic prophase. Specifically, we collected tissue at three time points post-RA injection: 8 dpi to enrich for zygotene to early pachytene, 13 dpi to enrich for midpachytene, and 16 dpi to increase the representation of late pachytene to diplotene transition (Figure 1; Supplemental Table S1). From each sample, we collected an average of ~3300 cells, with a total of 26,500 sequenced cells. After quality control filtering (see *Materials and Methods*), a total of 21,314 cells were retained across all datasets, with an average of ~1800 detected genes per cell. An unsupervised clustering analysis identified seven molecular clusters (Figure 4A), with each cluster consisting of cells from both genotypes and multiple time points (Figure 4B and Supplemental Figure S1B). A systematic comparison of the seven cluster centriods across the eight datasets confirmed the strong consistency of the identified cell types across the two genetic backgrounds and four developmental time points (Supplemental Figure S1A). Using the expression pattern of known cell type-specific markers (Chen *et al.*, 2018; Green *et al.*, 2018; Jung *et al.*, 2019), we annotated the seven major clusters as two germ cell types (spermatogonia and spermatocytes) and five somatic cell types (Sertoli, interstitial progenitor [Tcf21$^+$], immature Leydig, mature Leydig, and macrophages; see Figure 4C, Supplemental Figure S2, and Supplemental Table S2).

To identify changes in population dynamics and molecular changes during germ cell development and compare between the WT and the SCARKO testes, we reclustered only the germ cell populations, and obtained seven ordered subclusters (Figure 5A; Supplemental Table S3). According to the expression pattern of previously known meiosis stage-specific genes, these clusters correspond to undifferentiated spermatogonia (GC1), differentiating spermatogonia (GC2), leptotene/zygotene spermatocytes (GC3), early–mid-pachytene spermatocytes (GC4), late pachytene spermatocytes (GC5), diplotene spermatocytes (GC6), and early round spermatids (GC7) (Figure 5, A and B; Supplemental Table S3) (Chen *et al.*, 2018; Jung *et al.*, 2019). More mature germ cells were not expected since our collection was focused on juvenile testes. Although several markers are shared between undifferentiated and differentiated spermatogonia, others were more specific to either undifferentiated spermatogonia (GC1) or differentiating spermatogonia (GC2; e.g., *Gfra1* and *Zbtb16* in GC1 and *Stra8*, *Dmrt1* in GC2; see all markers

cells. (C) This panel shows representative SYCP1 (green) and SYCP3 (magenta) localization in pachytene spermatocytes isolated from WT (top) and SCARKO (bottom) testes. (D) Quantification of MLH1 foci in pachytene spermatocytes isolated from WT and SCARKO testes. The *x*-axis indicates the stages of pachytene cells isolated from synchronized testis. (E) This panel shows H1T-positive and -negative pachytene spermatocytes from WT and SACRKO testes. (F) This graph demonstrates similar frequency of H1T-positive spermatocytes from WT and SCARKO synchronized testes. The *x*-axis indicates the stages of pachytene cells isolated from synchronized testis. (G) This illustrates typical Giemsa-stained pachytene (top) and metaphase (bottom) spermatocytes after OA treatment. (H) The graph presents the percentage of metaphase cells among both WT and SCARKO spermatocytes after treatment with OA. The *x*-axis indicates both the treatment the cells were exposed to, as well as the prophase substage of the most advanced spermatocytes at the time of isolation. (NS, not significant; $^{**}P < 0.01$)

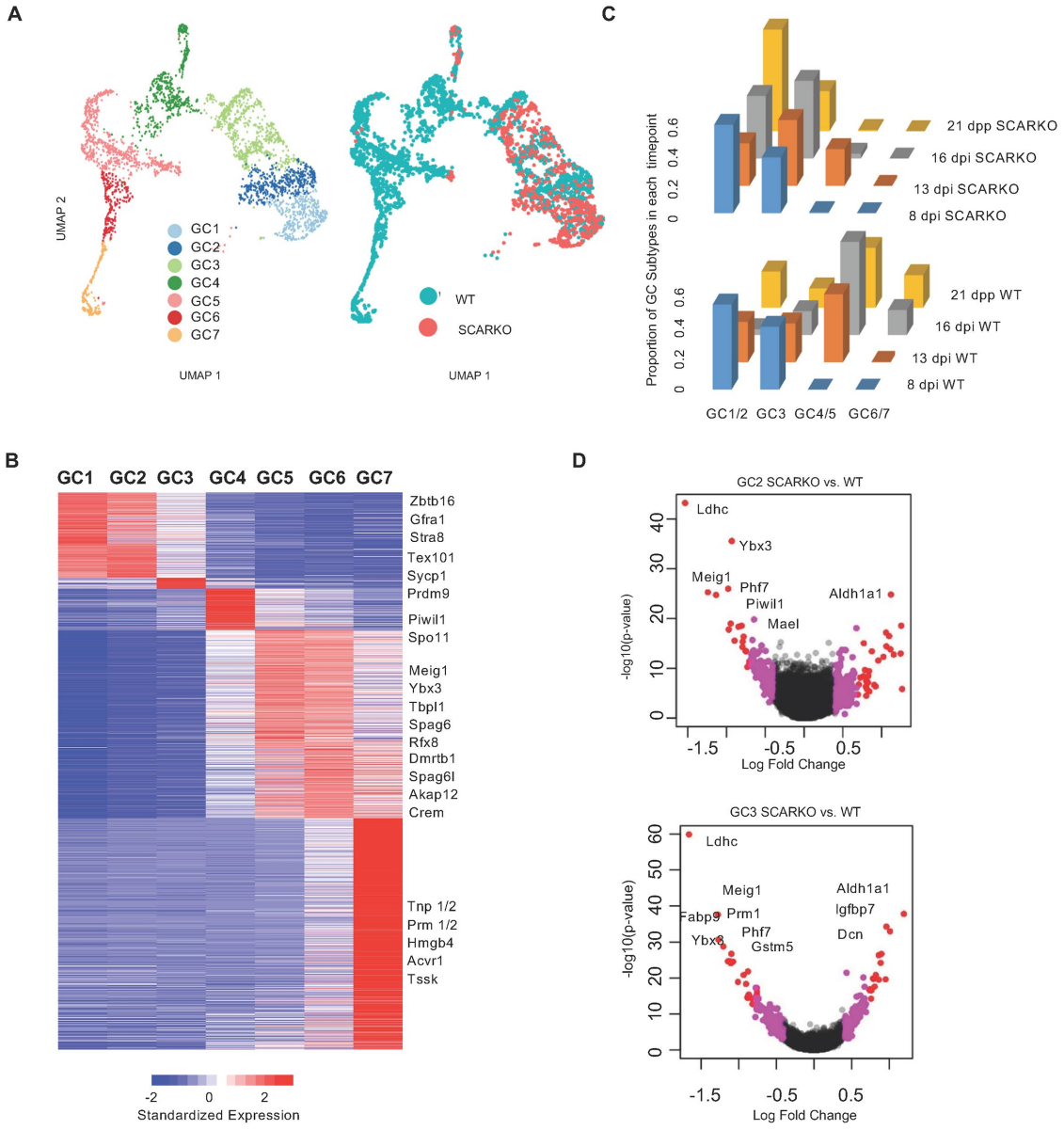

FIGURE 5: SCARKO germ-cell arrest occurs at the leptotene/zygotene to early–midpachytene transition. (A) Focused reclustering of ~3,100 germ cells, for both genotypes, identified seven ordered states, GC1-GC7. Cells in the UMAP plot are colored by cell state (left) or by genotype (right). The latter shows that SCARKO germ cells rarely advance to GC4. (B) Marker gene heatmap for the 7 states, with expression values for each gene standardized over the 7 cluster centroids. Representative genes are indicated on the right, for GC1, Undifferentiated SpG; GC2, Differentiated SpG; GC3. Leptotene/Zygotene; GC4; Early–midPachytene; GC5, Late Pachytene; GC6, Diplotene; GC7, Early Round Spermatids. **(C)** Distribution of germ cells over developmental states (collapsed from 7 to 5 states, shown from left to right), compared across two genotypes and 4 time points. The proportions of cells (y axis) shift to more matured states at later time points in WT, but fail to go beyond GC4/5 in SCARKO. (D) DE analysis between SCARKO and WT, shown as volcano plots, for GC2 (top) and GC3 (bottom). Select genes are indicated. Along the *x*-axis, pink indicates genes with 1.5- to 2-fold change, whereas red indicates >2-fold change.

in Supplemental Table S3). In the leptotene/zygotene stage (GC3) cluster, the spermatogonial cell transcriptional pattern is no longer dominant; instead, a distinct set of genes is up-regulated (Figure 5B and Supplemental Table S3). Among cells in the early–midpachytene cluster (GC4), further changes were observed in the transcriptome, with the spermatogonial transcriptional pattern being absent and many genes distinctively up-regulated, in a pattern continuing from pachytene through the diplotene transition, GC5-7 (Figure 5B; Supplemental Table S3).

To examine the differential contribution of the WT and SCARKO testes to the seven germ cell states, we labeled the germ cells in the UMAP projection based on genotype and observed that the majority of SCARKO germ cells did not exhibit transcriptomic progress beyond GC3, the transition from leptotene/zygotene to early–midpachytene stages (Figure 5A, right panel), with very few cells from SCARKO testes (32/800, 4%) reaching GC4, the early–midpachytene transcriptional state, compared with WT (461/2385, 19%). We further compared the proportion of cells over different germ cell

stages across the four developmental time points from the WT and mutant datasets. The majority of germ cells in SCARKO (top panel, Figure 5C) failed to advance beyond GC3 even in later time points such as 16 and 21 dpp, consistent with the UMAP view. In contrast, germ cells in WT (bottom panel, Figure 5C) were concentrated on GC1-3 at 8 dpi, but at later time points progressively shift to more mature stages. Hence, our scRNAseq analysis demonstrates that the SCARKO mutant germ cells mostly stall at an early pachytene *transcriptome* state, despite progressing to a midpachytene-like *cytological* state (Figures 2 and 3). This implies that the molecular/transcriptomic state is uncoupled from the cytological progress of the germ cells in SCARKO mutant testes.

To identify genes that might underlie the germ-cell arrest/loss in SCARKO mutants, we compared transcriptomes of GC2 and GC3 cells, which correspond to the stage prior to the arrest, between WT and SCARKO testes. We identified 50 and 52 genes that were at least twofold differentially expressed ($p < 0.01$) in GC2 and GC3 clusters, respectively, many or which were shared between the two time points (Figure 5D; Table 1), suggesting that misregulation begins in GC2. Among genes with lower expression in SCARKO were those previously known to be modulated by androgen signaling within the testes, such as *Fabp9* and *Gstm5* (De Gendt *et al.*, 2014). Other SCARKO down-regulated genes encode an RNA-binding protein (*Ybx3*) and proteins involved in cytoskeleton, acrosome, or cilia organization and formation (e.g., *Meig1, Spink2,* and *Rsph1),* which are important components for postmeiotic spermiogenic differentiation (Zhou *et al.*, 2010; Kott *et al.*, 2013; Snyder *et al.*, 2015; Zhang *et al.*, 2019). Genes up-regulated in SCARKO mutants included Aldh1a1, Igfbps, and mitochondrial membrane and oxidative phospohorylation transcripts. Furthermore, pathway analysis revealed that genes with lower expression in SCARKO at GC2 and GC3 are enriched for those involved in spermiogenesis and germ cell terminal differentiation, whereas those with higher expression in SCARKO are enriched for oxidative phosphorylation and mitochondrial protein transcripts (Supplemental Table S4). These observations suggest that in the absence of proper AR signaling in SCARKO, the germ cell development failed to advance beyond GC3 due to impared expression of a group of spermiogenesis transcripts, which are required for normal germ-cell progression from spermatogonia to midmeiotic to spermiogenic stages. The increased expression of mitochondrial and oxidative phosphorylation RNAs in SCARKO germ cells may be a secondary consequence of germ cell disruption or inability to repress oxidative phosphorylation in mutants. Whether these transcriptome dynamics have a permissive role, or an instructive or licensing role remains to be determined in the future.

Despite the much fewer GC4 cells in SCARKO, we compared their transcriptomes with the WT GC4 cells (Table 1; Supplemental Table S4) and found a lower expression of spermatid differentiation genes, suggesting that the SCARKO GC4 cells are functionally impaired, similar to GC2 and GC3. However, the escaping GC4 cells had an increase in ribosomal protein RNAs, suggesting heightened activity of protein production. Whether the heightened translation in a rare subpopulation of SCARKO germ cells enabled the progression beyond the GC3 state and/or the acquistion of competence to undergo chromosome condensation in response to OA treatment remains to be determined (Figure 3G).

Loss of functional Sertoli AR alters the transcriptome of Sertoli cells but not of other testicular somatic cells

In addition to soma-to-germ or germ-to-soma communication, the intercellular communication within the testis somatic compartment is important for maintaining tissue homeostasis and function. Therefore, we next examined how loss of AR signaling from Sertoli cells may affect the transcriptome of Sertoli cells themselves or those of other somatic cells in the testis. The merged WT and SCARKO datasets consisted of ~18,203 somatic cells: 12,373 in SCARKO and 5830 in WT mice (Figure 6A). Clustering analysis of the ~18,000 somatic cells revealed five clusters that are composed of well-mingled WT and SCARKO cells, which by marker gene analyses correspond to Sertoli cells, interstitial progenitors (*Tcf21*+, *Pdgfra*+), immature Leydig, mature Leydig, and macrophages (Figure 6, A and B; Supplemental Table S5). Interestingly, in addition to the expected higher relative abundance of somatic cells from the SCARKO mutants due to germ-cell loss in SCARKO, we find notable shifts in the population proportion between the WT and the SCARKO mutant testis (Figure 6C). Curiously, after correcting for the somatic cell number in the SCARKO mutant testis, there is a reduction in the number of mature Leydig cells and an increase in the number of immature and interstitail progenitor cells observed in the SCARKO testis (Figure 6C). Whether this is a result of aberrent signals from Sertoli cells to neighboring somatic cells or an indirect result of missing germ cell populations remains to be determined.

We then compared the transcriptomes of WT and SCARKO mutants in each of the five somatic cell types (Figure 6, A and B). However, we did not observe significant transcriptome differences in the somatic cell populations, namely macrophages, interstitial fibroblasts, and immature and adult Leydig cell populations (see Table 2). Next, the focused reclustering of Sertoli cells identified only a single cluster of well-mingled WT and SCARKO mutant cells, suggesting that Sertoli cells from the two genetic backgrounds are transcriptionally similar (Figure 6D; note that slight shifts in population are due to slightly higher cell size factor [#UMIs detected] in WT vs. SCARKO). The lack of global change in Sertoli cell molecular identity was further illustrated when examining the average expression of ubiquitously expressed Sertoli cell marker genes, that is, *Sox9, Amhr2*, and *Rhox8* (localized to the center of the volcano plot), indicating no significant differences in expression are observed between the two genotypes (Figure 6E). However, differential gene expression analysis identified 165 genes with at least twofold difference ($p < 1E-5$) between WT and SCARKO Sertoli cells (Table 2). One hundred twenty-two of these genes were down-regulated in SCARKO Sertoli cells, 65 of which have been reported in the literature to be androgen regulated, for example, *Tsx, Susd3, Rhox5, Serpina5, Drd4, Eppin, Clstn1, Esyt3*, and *Jam3,* including *Ar* itself, as expected (Lindsey and Wilkinson, 1996; Tan *et al.*, 2005; Willems *et al.*, 2010; De Gendt *et al.*, 2014) (Table 2). In contrast, 43 genes were up-regulated in SCARKO mutants and 12 overlapped with a previous publication (De Gendt *et al.*, 2014). Therefore, loss of AR in Sertoli cells leads to misregulation of a small number of genes, which explains the lack of global transcriptome changes in the Sertoli cell population in SCARKO mutants. Taken together, our scRNA analysis revealed a discrete molecular fingerprint of AR-regulated genes in Sertoli cells, including known and previously unknown genes.

DISCUSSION

This study investigated the mechanistic basis on which androgen signaling in Sertoli cells instructs progression of germ cells meiosis. Specifically, we exploited the SCARKO model coupled with synchronization of spermatogenesis in juvenile mice (Figure 1; Supplemental Table S1) and scRNAseq analyses of the juvenile testis. Our cytological analysis of SCARKO mutant testis shows extensive germ-cell loss at all stages of germ cell development (Figure 2), suggesting that AR signaling profoundly affects testicular homeostasis.

A. Markers differentially expressed between SCARKO and WT in GC2-DiffSPG					
Gene	**p_val**	**avg_logFC**	**pct.1**	**pct.2**	**p_val_adj**
Ldhc	6.1E-44	–1.53	6.6%	78.0%	2.0E-39
Meig1	2.7E-36	–0.93	8.3%	70.6%	9.0E-32
Crisp2	1.0E-26	–0.98	2.5%	49.8%	3.4E-22
Rbakdn	5.3E-26	–1.24	3.3%	54.5%	1.8E-21
Sparc	1.6E-25	1.12	59.5%	42.4%	5.2E-21
Ropn1l	1.8E-25	–1.13	4.1%	55.7%	5.8E-21
Fam229b	1.1E-19	–0.95	4.1%	47.7%	3.6E-15
Rsph1	2.8E-19	–0.80	9.1%	54.2%	9.1E-15
Gstm2	2.8E-19	1.25	44.6%	13.3%	9.2E-15
Smim24	4.4E-19	–0.85	3.3%	44.3%	1.4E-14
Fabp9	1.6E-18	–0.97	5.0%	46.4%	5.4E-14
Aldh1a1	6.9E-18	1.06	55.4%	36.2%	2.3E-13
Malat1	3.5E-17	1.10	89.3%	93.2%	1.1E-12
Pgam2	4.5E-17	–0.78	0.0%	32.8%	1.5E-12
Cox8c	2.9E-16	–0.90	9.1%	50.5%	9.4E-12
1700008K24Rik	4.6E-16	–0.79	0.8%	34.4%	1.5E-11
Maged1	9.5E-16	0.77	34.7%	39.3%	3.1E-11
Hsd3b6	3.9E-15	1.06	38.0%	20.4%	1.3E-10
Hspb9	5.5E-15	–0.79	0.8%	33.1%	1.8E-10
Clu	1.5E-14	1.11	41.3%	23.2%	5.1E-10
Asrgl1	3.3E-14	–0.75	10.7%	49.8%	1.1E-09
Gm37376	3.9E-14	0.87	47.9%	26.6%	1.3E-09
Pdcl2	3.9E-14	–0.75	2.5%	35.3%	1.3E-09
Defb19	1.1E-13	1.25	41.3%	19.2%	3.6E-09
Gstm1	1.8E-13	1.16	43.0%	19.2%	5.8E-09
Apoe	5.0E-13	1.02	38.8%	27.6%	1.6E-08
Igfbp7	2.8E-12	0.96	38.0%	21.1%	9.1E-08
Clgn	3.7E-12	–0.70	10.7%	46.1%	1.2E-07
Dkkl1	7.5E-12	–0.70	4.1%	35.0%	2.5E-07
Ppp3r2	2.3E-11	–0.71	0.8%	26.6%	7.5E-07
Spata33	5.5E-11	–0.73	13.2%	47.7%	1.8E-06
Acsbg1	2.2E-10	0.79	23.1%	7.1%	7.3E-06
Tuba1a	3.7E-10	0.84	12.4%	5.9%	1.2E-05
Erdr1	3.5E-09	0.83	37.2%	21.7%	1.2E-04
Fxyd1	4.2E-09	0.76	15.7%	4.3%	1.4E-04
Hsd3b1	7.9E-09	0.72	23.1%	20.4%	2.6E-04
Neat1	4.0E-08	0.80	19.0%	11.5%	1.3E-03
Mgp	4.2E-08	0.81	26.4%	9.3%	1.4E-03
Akr1cl	7.9E-08	0.82	39.7%	23.5%	2.6E-03
Nenf	1.7E-07	0.71	16.5%	6.2%	5.7E-03
Cst12	2.2E-07	0.90	17.4%	9.6%	7.3E-03
Ldhb	4.3E-07	0.92	19.8%	9.9%	1.4E-02
Cst9	4.9E-07	0.80	20.7%	10.2%	1.6E-02
Mgst1	1.5E-06	0.81	20.7%	10.2%	4.8E-02
Aard	1.5E-06	1.26	19.0%	7.7%	5.0E-02
Defb36	4.3E-06	0.84	8.3%	2.8%	1.4E-01
Rhox8	1.9E-05	0.69	9.1%	4.3%	6.2E-01
Tmsb4x	3.4E-05	0.80	24.0%	16.1%	1.0E+00

TABLE 1: Genes differentially expressed between WT and SCARKO in three of the germ cell developmental stages (GC2-4).

(Continues)

B. Genes differentially expressed between SCARKO and WT in GC3: leptotene/zygotene spermatocytes					
Gene	**p_val**	**avg_logFC**	**pct.1**	**pct.2**	**p_val_adj**
Ldhc	1.3E-60	–1.66	19.9%	68.7%	4.3E-56
Apoe	1.3E-38	1.19	77.1%	35.3%	4.4E-34
Meig1	2.3E-38	–1.28	27.7%	66.9%	7.7E-34
Aldh1a1	4.7E-35	0.96	76.2%	39.3%	1.5E-30
Gstm1	9.8E-34	1.01	70.5%	30.8%	3.2E-29
Crisp2	2.1E-31	–1.27	6.3%	39.3%	7.0E-27
Rbakdn	1.6E-29	–1.21	6.0%	40.4%	5.4E-25
Spink2	1.7E-27	–1.10	3.3%	34.3%	5.7E-23
Gstm2	1.9E-27	0.89	62.3%	22.8%	6.2E-23
Igfbp7	4.6E-27	0.86	68.4%	31.3%	1.5E-22
Ropn1l	2.1E-25	–1.14	16.0%	46.6%	7.0E-21
Fabp9	2.2E-25	–1.12	18.1%	52.4%	7.1E-21
1700008K24Rik	2.9E-25	–1.08	7.8%	41.1%	9.4E-21
Fam229b	3.0E-25	–1.08	12.0%	42.9%	9.9E-21
Akr1cl	6.0E-25	0.88	67.2%	32.6%	2.0E-20
Dkkl1	7.8E-25	–1.10	6.3%	35.3%	2.6E-20
Lyar	1.5E-22	–0.88	37.7%	65.4%	4.9E-18
Mgp	1.4E-21	0.82	53.9%	19.5%	4.5E-17
Cox8c	1.4E-21	–0.94	24.1%	49.6%	4.8E-17
Hmgcs2	1.4E-20	0.78	54.2%	20.6%	4.6E-16
Defb19	1.8E-20	0.79	62.0%	27.1%	5.8E-16
Dcn	2.3E-20	0.95	48.5%	17.3%	7.4E-16
Agt	2.9E-20	0.86	33.4%	7.0%	9.5E-16
Ybx3	1.2E-19	–1.01	13.3%	37.8%	4.0E-15
Hspb9	4.4E-19	–0.90	1.8%	23.6%	1.5E-14
Hsd3b6	2.4E-18	0.80	55.1%	24.8%	8.0E-14
Hrasls5	5.5E-18	–0.78	0.9%	19.8%	1.8E-13
Cetn1	5.9E-18	–0.76	3.0%	24.3%	1.9E-13
Clu	1.3E-17	0.74	56.9%	26.6%	4.3E-13
Apoc1	2.4E-17	0.74	25.3%	4.3%	8.0E-13
Igfbp6	2.8E-17	0.76	41.3%	12.8%	9.2E-13
Pgam2	7.3E-17	–0.76	2.1%	22.3%	2.4E-12
Gstm5	3.7E-16	–0.87	16.3%	40.6%	1.2E-11
Phf7	5.5E-16	–0.76	31.0%	57.1%	1.8E-11
Gm5617	2.3E-15	–0.88	12.3%	35.8%	7.6E-11
Cmtm2b	2.8E-15	–0.77	2.7%	20.6%	9.4E-11
Asrgl1	3.4E-15	–0.88	13.9%	38.3%	1.1E-10
Ggnbp1	4.3E-15	–0.83	6.3%	27.1%	1.4E-10
Ppp3r2	5.6E-15	–0.74	1.8%	19.8%	1.9E-10
Chchd10	5.8E-15	0.76	46.4%	20.6%	1.9E-10
Rsph1	9.0E-15	–0.75	33.1%	60.9%	3.0E-10
Ccdc38	1.6E-13	–0.76	1.8%	16.5%	5.3E-09
Smim24	1.6E-13	–0.82	12.0%	32.3%	5.3E-09
Pabpc2	4.5E-13	–0.72	1.5%	17.0%	1.5E-08

TABLE 1: Genes differentially expressed between WT and SCARKO in three of the germ cell developmental stages (GC2-4).

(Continues)

B. Genes differentially expressed between SCARKO and WT in GC3: leptotene/zygotene spermatocytes					
Gene	**p_val**	**avg_logFC**	**pct.1**	**pct.2**	**p_val_adj**
AA467197	2.1E-12	–0.76	13.3%	34.8%	6.9E-08
Ldhal6b	5.0E-12	–0.76	4.5%	21.6%	1.6E-07
Pdcl2	5.7E-12	–0.76	11.1%	31.3%	1.9E-07
Prm1	9.8E-12	–0.72	1.2%	15.0%	3.2E-07
Spata4	1.1E-11	–0.71	5.1%	23.1%	3.7E-07
Piwil1	6.9E-10	–0.78	6.6%	22.6%	2.3E-05
C. Markers differentially expressed between SCARKO and WT in C4-EmPachy					
Gene	**p_val**	**avg_logFC**	**pct.1**	**pct.2**	**p_val_adj**
Aldh1a1	4.6E-16	1.24	93.8%	44.5%	1.5E-11
Rps29	8.5E-14	1.04	93.8%	45.3%	2.8E-09
Rps27	1.7E-13	1.05	96.9%	49.7%	5.8E-09
Gstm1	3.2E-13	1.13	90.6%	29.7%	1.1E-08
Rps14	7.6E-13	0.82	90.6%	67.2%	2.5E-08
Gstm2	8.7E-13	1.20	84.4%	25.6%	2.9E-08
Apoe	8.8E-13	1.15	90.6%	35.6%	2.9E-08
Rps21	1.3E-12	0.92	93.8%	56.8%	4.3E-08
Mgp	1.4E-12	1.20	81.2%	24.1%	4.5E-08
Cst3	1.8E-12	0.98	93.8%	55.7%	6.0E-08
Aldh2	4.7E-12	1.05	65.6%	13.9%	1.5E-07
Rps26	7.3E-11	0.94	90.6%	53.1%	2.4E-06
Dcn	2.0E-10	0.85	87.5%	27.8%	6.4E-06
Igfbp7	3.0E-10	1.04	87.5%	30.4%	9.9E-06
Ndufa3	3.4E-10	0.96	81.2%	28.0%	1.1E-05
Rpl23	5.8E-10	0.75	96.9%	50.5%	1.9E-05
Rpl12	9.2E-10	0.86	90.6%	41.6%	3.0E-05
Rpl39	1.2E-09	0.98	78.1%	24.5%	3.9E-05
Ifi27l2a	1.3E-09	0.87	65.6%	13.7%	4.3E-05
Defb19	1.3E-09	0.91	84.4%	30.2%	4.4E-05
Sod1	1.5E-09	0.83	84.4%	28.2%	4.9E-05
Fxyd1	1.6E-09	0.78	71.9%	17.6%	5.4E-05
Pltp	3.0E-09	0.77	56.2%	10.0%	9.9E-05
Rplp1	3.3E-09	0.80	93.8%	62.9%	1.1E-04
Tmsb4x	3.5E-09	0.72	87.5%	31.2%	1.2E-04
Rps12	3.8E-09	0.86	81.2%	51.2%	1.2E-04
Id3	4.8E-09	0.85	68.8%	16.7%	1.6E-04
Rps19	7.5E-09	0.78	90.6%	36.2%	2.5E-04
Rps15a	8.1E-09	0.87	93.8%	50.8%	2.7E-04
Hsd3b6	8.2E-09	0.85	84.4%	29.7%	2.7E-04
Rpl41	9.8E-09	0.78	96.9%	64.2%	3.2E-04
Serping1	1.0E-08	0.73	59.4%	10.8%	3.3E-04
Aebp1	1.0E-08	0.77	62.5%	12.8%	3.3E-04
Rpl38	1.0E-08	0.82	84.4%	37.1%	3.4E-04
Fabp3	1.1E-08	0.70	75.0%	20.8%	3.5E-04
Lyz2	1.1E-08	0.78	71.9%	18.9%	3.6E-04

TABLE 1: Genes differentially expressed between WT and SCARKO in three of the germ cell developmental stages (GC2-4).

(Continues)

C. Markers differentially expressed between SCARKO and WT in C4-EmPachy					
Gene	**p_val**	**avg_logFC**	**pct.1**	**pct.2**	**p_val_adj**
Uqcr11	1.8E-08	0.77	84.4%	29.5%	5.9E-04
Col1a2	1.8E-08	0.86	71.9%	19.5%	5.9E-04
Rps9	1.8E-08	0.90	90.6%	46.4%	6.0E-04
Rps28	2.1E-08	0.96	75.0%	36.7%	7.0E-04
Rpl36	2.7E-08	0.79	93.8%	47.7%	9.0E-04
Cox6b1	3.7E-08	0.78	75.0%	23.0%	1.2E-03
B2m	4.3E-08	0.74	75.0%	23.0%	1.4E-03
Rpl37	7.8E-08	0.88	84.4%	43.2%	2.6E-03
Cd81	9.9E-08	0.76	62.5%	15.2%	3.3E-03
Rpl37a	1.6E-07	0.86	84.4%	45.6%	5.4E-03
Vim	1.7E-07	0.78	59.4%	14.3%	5.6E-03
Acaa2	1.8E-07	0.82	65.6%	17.8%	6.0E-03
Cpe	2.0E-07	0.75	68.8%	19.5%	6.5E-03
Rpl34	2.0E-07	0.80	84.4%	34.3%	6.7E-03
Sepp1	2.1E-07	0.74	65.6%	19.1%	6.9E-03
Rpl31	2.2E-07	0.72	93.8%	51.8%	7.4E-03
Hsd3b1	2.6E-07	0.76	71.9%	22.6%	8.6E-03
Cox7b	4.7E-07	0.73	59.4%	15.4%	1.5E-02
Fth1	1.0E-06	0.69	87.5%	59.0%	3.5E-02
1810022K09Rik	1.1E-06	0.69	62.5%	16.9%	3.6E-02
Rpl35a	1.9E-06	0.83	78.1%	34.3%	6.1E-02
Rps23	2.1E-06	0.70	84.4%	46.4%	6.8E-02
Clu	2.1E-06	0.75	71.9%	28.6%	6.9E-02
Tpt1	2.1E-06	0.72	78.1%	38.2%	7.1E-02
Acsbg1	2.2E-06	0.73	65.6%	21.5%	7.2E-02
Agt	3.0E-06	0.71	59.4%	16.5%	9.8E-02
Atp5e	3.0E-06	0.70	87.5%	43.4%	1.0E-01
Aldh1a7	3.2E-06	0.70	40.6%	7.2%	1.1E-01
Rpsa	3.3E-06	0.76	78.1%	33.4%	1.1E-01
Cox7c	8.3E-06	0.72	84.4%	47.5%	2.7E-01
Rpl36a	1.0E-05	0.76	59.4%	18.4%	3.4E-01
Akr1cl	1.7E-05	0.69	78.1%	34.7%	5.6E-01
Sh3bgrl3	7.7E-04	0.70	37.5%	12.1%	1.0E+00

For each stage (G2, GC3, or GC4), the significantly expressed genes are listed in the table. Genes are filtered by twofold change to either direction, where a negative value of avg_logFC means lower expression in SCARKO. FC is in natural log scale; pct.1 is the percentage of cells in SCARKO in which the gene is detected.

TABLE 1: Genes differentially expressed between WT and SCARKO in three of the germ cell developmental stages (GC2-4). Continued

Furthermore, we show that androgen signaling in Sertoli cells is not essential for major chromosomal events of meiotic prophase, including chromosome synapsis, reciprocal recombination, and expression of midpachytene markers that precede acquisition of competence for the meiotic division phase (Figure 3, A–F). Despite an apparent normal meiotic progression, pachytene SCARKO spermatocytes fail to acquire competence to enter the division phase and instead stall in a pachytene-like histological state (Figure 3, G and H). Our scRNAseq confirmed the meiotic arrest phenotype, but also revealed a unexpected disconnect in germ cell cytological state versus molecular state (Figures 4 and 5). Although the SCARKO mutant germ cells reach a pachytene-like state histologically, they arrest at a leptotene or zygotene transcriptome state. Many of the genes that fail to activate in SCARKO mutant germ cells are involved in spermiogenesis, suggesting that AR-induced signaling in Sertoli provides an environment conducive for midprophase spermatocytes to undergo meiotic division and embark on spermiogenic differentiation. In the somatic compartment of SCARKO mutants, we identified several AR-regulated genes in Sertoli cells but did not observe any transcriptional changes in neighboring somatic cells. In

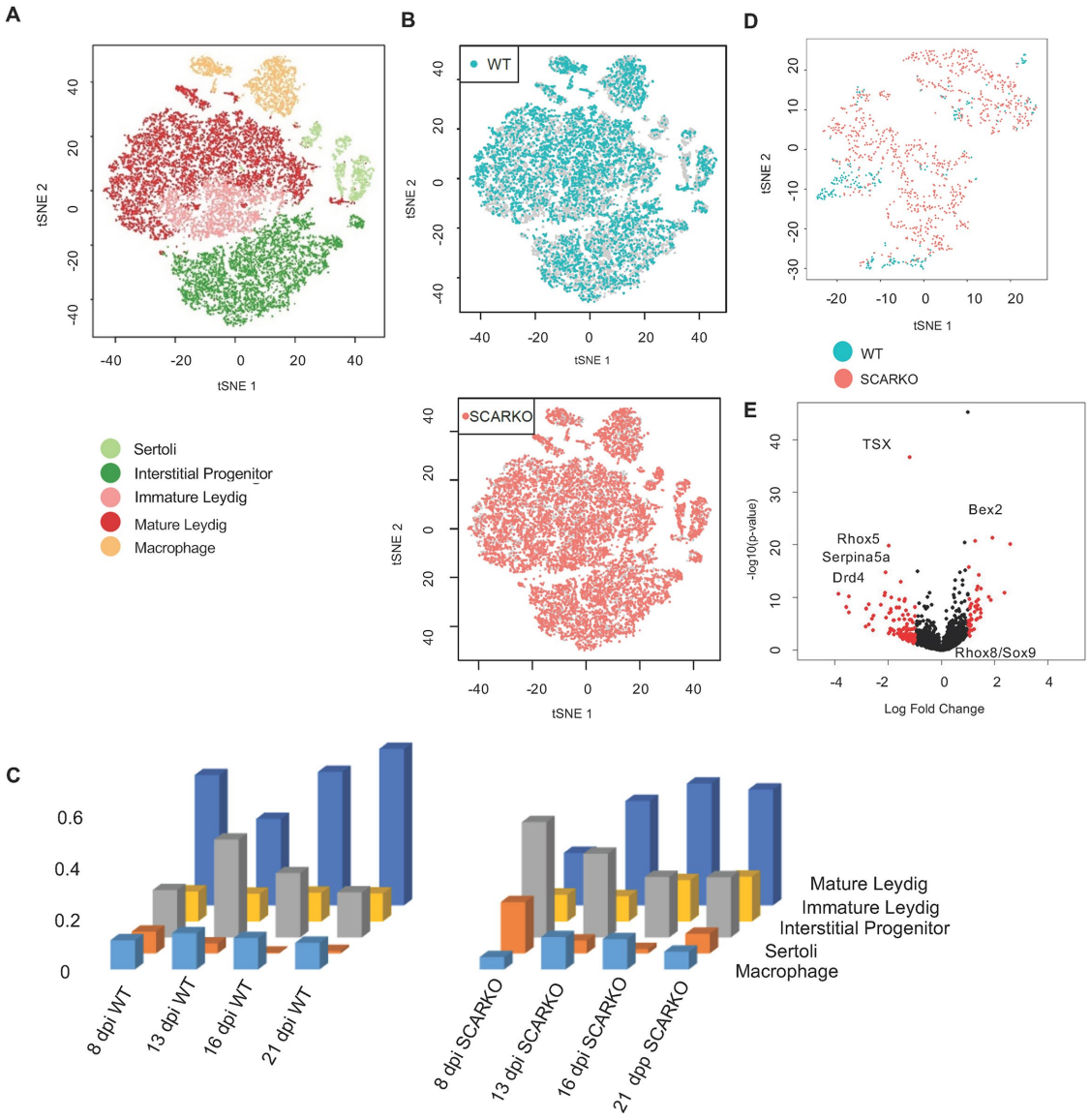

FIGURE 6: Loss of functional Sertoli AR affects relative proportion of somatic cells and alters the transcriptome of Sertoli cells. (A) Focused reclustering of ~18,000 somatic cells confirms the five major somatic cell types. (B) Same visualization as in A, but colored by genotype, showing that cells from the two genotypes occupy comparable tSNE space. (C) Distribution of somatic cells, shown as percentages (y axis) of the 5 cell types, compared over two genotypes and 4 time points (left to right). (D) Focused tSNE projection of Sertoli cells, colored by genotype. (E) DE analysis of Sertoli cells between SCARKO and WT, shown as volcano plot with red indicates >1.5-fold change. Select genes are indicated.

all, our approach enabled us to uncover important germ cell intrinsic and extrinsic features required for proper germ-cell progression.

Loss of functional Sertoli AR alters the transcriptome of Sertoli cells

Our differential scRNAseq analysis identified 165 genes misregulated in SCARKO Sertoli cells (Table 2). Of those genes, 77 were previously reported by de Gendt *et al.* (2014) and previously associated with male infertility or subfertility when gene function is abrogated, suggesting biological significance for the set of 165 genes. For example, *Tsx* mutant mice are subfertile and have an increase in apoptotic pachytene cells (Anguera *et al.*, 2011), while *Bsg* KO animals are sterile due to impaired interaction between germ cells and Sertoli cells (Bi *et al.*, 2013). In addition, *Serpina5* mutant mice exhibit compromised blood–testis barrier function (Uhrin *et al.*, 2000), a phenomenon also noted in SCARKO mutants. Given that many of the 165 genes lead to infertility in a loss of function context, we hypothesize that gene combinations may contribute to diminished function of SCARKO Sertoli cells and infertility in SCARKO animals. Interestingly, few transcriptional differences were observed in the neighboring somatic cell types. This suggests that loss of androgen signaling within juvenile Sertoli cells has no gross immediate transcriptional effects on the environment surrounding the seminiferous tubules. However, our Drop-seq data suggest that the SCARKO testes have fewer mature Leydig cells and an accumulation of interstitial progenitor and immature Leydig cells. Although at first glance it appears to be inconsistent with an earlier report showing that loss of AR signaling in the testis had no effect on Leydig cell

A. Genes differentially expressed between SCARKO and WT in Sertoli cells				
Gene	**FC(log2)**	***P* val**	**%SCARKO**	**%WT**
Rhox5	–3.86	2.0E-11	2.10%	35.30%
Anxa9	–3.57	5.7E-09	1.80%	25.70%
Drd4	–3.48	7.1E-11	2.50%	34.00%
Defb45	–3.48	6.8E-08	3.30%	28.20%
Zcchc18	–2.84	3.0E-05	2.00%	19.10%
Gm648	–2.83	1.2E-08	3.90%	29.90%
Gja6	–2.73	2.2E-09	3.00%	29.90%
Gpr179	–2.73	1.2E-05	1.40%	16.60%
Cdkn1a	–2.62	9.3E-07	3.90%	26.60%
Cdkn2b	–2.58	1.5E-04	2.00%	16.60%
Ar	–2.56	2.4E-07	4.50%	29.50%
Clstn1	–2.27	2.7E-09	6.00%	35.70%
Emb	–2.14	3.8E-11	7.40%	40.70%
Tsx	–2.12	1.4E-11	14.40%	53.10%
Serpina5	–2.10	1.8E-15	11.50%	48.50%
Gadd45g	–2.08	5.7E-07	5.90%	28.60%
1700024P16Rik	–1.98	5.9E-04	3.40%	20.30%
Susd3	–1.97	1.4E-20	20.80%	65.60%
Slc7a4	–1.97	7.0E-08	8.70%	41.50%
Nrn1l	–1.93	3.1E-04	2.60%	15.40%
Porcn	–1.92	7.2E-05	3.00%	19.50%
Atp13a2	–1.91	1.6E-08	9.50%	38.60%
Gm3880	–1.90	4.4E-08	8.90%	36.90%
Rnf128	–1.89	1.0E-04	4.40%	20.30%
Eppin	–1.88	1.1E-10	13.70%	50.20%
Igsf8	–1.85	1.1E-04	4.50%	21.20%
Smim10l2a	–1.81	1.9E-06	5.20%	28.60%
P2rx2	–1.79	1.9E-06	8.90%	32.80%
Slc41a2	–1.79	1.9E-04	4.30%	20.70%
Tmem52	–1.78	9.5E-04	1.50%	16.60%
Lrp8	–1.69	8.6E-09	11.10%	39.40%
1700019B21Rik	–1.65	5.4E-04	8.30%	21.60%
Akap17b	–1.60	1.3E-04	5.40%	26.10%
Derl3	–1.59	8.7E-09	11.10%	40.20%
Kctd13	–1.59	1.2E-06	8.40%	32.00%
Esyt3	–1.58	2.4E-10	12.10%	46.10%
Tbc1d8	–1.57	1.2E-04	4.50%	20.70%
Slc38a5	–1.56	9.1E-04	5.10%	17.00%
Syne1	–1.56	9.4E-04	3.00%	16.20%
Gpd1	–1.56	9.0E-04	2.20%	16.20%
Dmwd	–1.55	2.3E-03	4.10%	15.80%
Nfatc2ip	–1.53	9.6E-14	19.60%	61.00%
Tbx22	–1.52	2.4E-04	6.00%	22.40%

TABLE 2: Genes differentially expressed between SCARKO and WT in five somatic cell types.

(Continues)

A. Genes differentially expressed between SCARKO and WT in Sertoli cells				
Gene	**FC(log2)**	***P* val**	**%SCARKO**	**%WT**
Bcl2l11	−1.51	6.9E-04	4.70%	18.70%
Cd24a	−1.48	1.2E-03	6.70%	23.20%
Cyp2d22	−1.48	1.6E-03	5.20%	19.90%
Rora	−1.46	5.1E-03	4.00%	17.40%
Pdcl	−1.45	6.7E-03	6.20%	15.80%
Jam3	−1.45	2.0E-07	12.40%	41.90%
Pim3	−1.43	1.0E-03	4.90%	19.10%
Mccc2	−1.43	9.6E-05	7.40%	26.10%
Bend4	−1.41	9.6E-04	3.10%	17.80%
B4galt6	−1.41	6.6E-05	5.40%	24.50%
Tpd52l1	−1.39	1.3E-06	12.60%	39.80%
Cd302	−1.39	4.6E-10	20.10%	51.90%
mt-Ty	−1.37	3.2E-03	5.10%	17.00%
Syt7	−1.37	1.0E-03	7.00%	22.80%
Gas2l1	−1.37	1.8E-10	23.70%	63.10%
Cotl1	−1.34	7.1E-04	6.20%	22.80%
Slc4a5	−1.34	4.5E-03	4.40%	16.60%
Slc3a2	−1.33	2.7E-08	21.90%	53.90%
Gm26917	−1.33	8.4E-04	8.80%	21.60%
Notch1	−1.32	2.9E-04	9.10%	25.70%
Fbxl14	−1.32	8.5E-03	3.60%	15.40%
Mageb16	−1.31	2.8E-05	9.00%	33.20%
Hopx	−1.30	9.7E-06	10.60%	35.30%
Tomm40l	−1.30	1.1E-02	5.50%	15.40%
Rab4a	−1.30	1.8E-03	7.10%	19.90%
Cited4	−1.29	1.5E-04	9.90%	33.60%
Cmip	−1.29	6.0E-03	4.10%	17.00%
Per1	−1.29	6.1E-03	5.30%	19.10%
Phactr4	−1.27	3.3E-03	5.40%	18.30%
Plp1	−1.25	1.4E-07	21.80%	48.10%
Megf8	−1.24	6.5E-03	6.20%	22.80%
Mbd6	−1.23	9.4E-03	6.10%	17.00%
Lhfp	−1.22	1.9E-02	5.60%	17.80%
Pfkl	−1.22	1.0E-04	9.10%	32.40%
Pbld2	−1.22	1.0E-03	4.50%	22.80%
Ubac2	−1.20	1.4E-06	12.20%	37.80%
mt-Rnr2	−1.20	2.4E-37	100.00%	100.00%
Zfyve19	−1.19	1.0E-02	5.20%	15.40%
Alg14	−1.19	1.3E-02	6.10%	16.60%
Alg5	−1.18	7.0E-04	8.90%	26.60%
Cers6	−1.18	4.1E-03	5.50%	17.80%
Cdc42se2	−1.17	1.3E-04	11.30%	32.80%
Gm23935	−1.16	7.4E-04	10.40%	27.00%

TABLE 2: Genes differentially expressed between SCARKO and WT in five somatic cell types.

(Continues)

A. Genes differentially expressed between SCARKO and WT in Sertoli cells				
Gene	**FC(log2)**	***P* val**	**%SCARKO**	**%WT**
Pdik1l	−1.16	8.4E-03	5.00%	17.40%
Vsig1	−1.14	1.4E-06	16.30%	42.30%
Nxnl2	−1.14	9.7E-05	9.60%	32.40%
Slc25a13	−1.14	3.0E-03	6.00%	20.70%
Arl8a	−1.13	1.4E-03	9.40%	26.60%
Ncapd2	−1.12	5.7E-03	5.90%	17.80%
March6	−1.11	1.7E-02	6.40%	17.00%
Asb7	−1.10	9.9E-04	9.90%	24.90%
Bop1	−1.10	1.6E-02	5.70%	16.60%
Golm1	−1.10	2.0E-03	10.30%	26.60%
Trf	−1.09	3.0E-03	6.40%	21.60%
Timm10	−1.08	9.8E-05	18.40%	44.40%
Fam3a	−1.08	1.2E-02	3.40%	15.80%
mt-Nd3	−1.07	4.4E-06	14.70%	44.40%
Ube2a	−1.06	2.8E-03	9.60%	21.60%
Xpot	−1.06	4.5E-02	6.00%	16.60%
Dmpk	−1.06	2.2E-03	7.60%	24.10%
Itpr2	−1.05	1.7E-03	7.80%	24.10%
Sgk1	−1.04	2.6E-02	7.00%	17.00%
Gipc1	−1.03	2.0E-02	7.10%	15.80%
Gle1	−1.03	2.6E-02	5.60%	16.20%
Micall2	−1.03	1.4E-02	4.70%	16.20%
Sulf2	−1.02	8.4E-03	9.60%	24.90%
Capn10	−1.02	1.2E-02	7.40%	22.00%
Gm4980	−1.02	2.9E-03	9.40%	25.30%
Twf2	−1.02	8.2E-03	8.80%	22.40%
Rmdn3	−1.02	3.9E-03	7.30%	22.80%
Smox	−1.01	1.4E-03	14.10%	32.40%
Paqr7	−1.01	5.8E-05	13.50%	34.90%
Atp8a1	−1.01	2.2E-02	5.40%	17.80%
Atp6ap1	−1.01	9.7E-04	11.70%	31.50%
Lamtor3	−1.00	2.0E-03	8.80%	24.90%
Sod3	−1.00	5.9E-09	25.70%	57.70%
Fam84a	−1.00	8.5E-03	7.70%	23.20%
Nxf3	−1.00	2.8E-07	25.00%	61.00%
Mrpl19	−1.00	1.1E-02	9.10%	20.30%
Dnajc19	1.00	1.2E-05	21.40%	21.20%
Mt3	1.01	2.3E-06	25.10%	22.80%
Suclg2	1.02	3.4E-06	24.00%	22.40%
Myl6	1.03	1.9E-16	59.00%	51.00%
Usp3	1.03	4.8E-04	16.90%	17.00%
Mrpl48	1.04	2.5E-05	18.70%	19.10%
Usp53	1.05	7.4E-06	22.30%	22.40%

TABLE 2: Genes differentially expressed between SCARKO and WT in five somatic cell types.

(Continues)

A. Genes differentially expressed between SCARKO and WT in Sertoli cells				
Gene	**FC(log2)**	***P* val**	**%SCARKO**	**%WT**
Cnn3	1.05	2.2E-10	39.60%	32.80%
Ildr2	1.06	1.8E-03	16.00%	11.20%
Plcg1	1.07	1.5E-04	19.40%	14.10%
Me2	1.08	1.0E-08	37.50%	29.90%
Aldh1a2	1.08	3.6E-09	27.10%	18.30%
Wfdc9	1.09	1.4E-07	26.00%	24.90%
Gm5835	1.09	2.2E-05	19.40%	16.60%
Ccni	1.09	1.8E-07	26.40%	20.30%
Plce1	1.10	1.2E-06	23.50%	26.10%
Trip6	1.11	1.7E-05	19.70%	17.40%
Pcp4l1	1.12	9.5E-07	22.70%	22.80%
Ltbp4	1.13	1.6E-06	18.90%	14.10%
Hs6st2	1.13	1.6E-09	40.10%	32.80%
Wwtr1	1.16	1.6E-04	16.50%	11.60%
Dab2ip	1.23	1.0E-04	15.70%	10.40%
Grcc10	1.24	5.1E-08	23.10%	18.70%
Bex2	1.26	1.7E-21	49.60%	46.10%
Prkar2a	1.27	4.7E-09	28.70%	23.70%
Cpne8	1.31	1.6E-06	21.20%	14.10%
Ptprf	1.31	6.4E-10	31.00%	24.10%
Dst	1.33	3.1E-12	29.80%	18.30%
Il17re	1.34	9.8E-07	15.20%	13.30%
Shisa8	1.35	1.4E-08	24.90%	18.30%
Pitrm1	1.36	3.2E-09	23.00%	19.90%
H2-Q10	1.37	7.4E-13	33.30%	24.10%
Oaz1-ps	1.39	2.7E-10	26.80%	19.50%
Nudt19	1.41	5.6E-15	37.90%	27.80%
Aass	1.46	4.4E-07	16.10%	12.00%
Pdlim4	1.47	1.6E-08	21.80%	13.70%
Gstm2-ps1	1.48	7.0E-08	20.20%	14.10%
Jun	1.48	2.2E-12	28.00%	22.80%
Tnfrsf12a	1.77	8.6E-11	22.40%	9.50%
Arhgap21	1.85	2.9E-10	17.90%	11.20%
Oxct1	1.92	4.5E-22	32.40%	19.90%
4930486L24Rik	2.36	1.4E-11	15.30%	5.40%
Cxxc5	2.58	6.8E-21	23.40%	6.60%
B. Genes differentially expressed between SCARKO and WT in mature Leydig cells				
Gene	**FC(log2)**	***P* val**	**%SCARKO**	**%WT**
Adamts5	−1.10	1.2E-50	20.10%	13.60%
Cst12	−1.00	4.1E-48	27.20%	30.80%
Wfdc10	−1.00	1.0E-35	14.20%	15.50%
Ces1d	1.19	5.0E-77	43.10%	24.90%
Nr4a1	1.23	4.0E-51	29.50%	10.40%

TABLE 2: Genes differentially expressed between SCARKO and WT in five somatic cell types.

(Continues)

C. Genes differentially expressed between SCARKO and WT in immature Leydig				
Gene	**FC(log2)**	***P* val**	**%SCARKO**	**%WT**
Cst12	–1.23	6.0E-39	34.30%	36.70%
Wfdc10	–1.21	1.2E-18	17.90%	19.00%
Cst9	–1.21	1.0E-21	29.60%	32.00%
Col13a1	–1.18	1.4E-08	10.50%	19.30%
Lbh	–1.15	1.4E-08	10.10%	18.00%
Gm5687	–1.05	1.7E-06	10.20%	17.80%
Sox4	–1.03	2.1E-07	11.10%	16.70%
Spon1	1.02	1.3E-10	27.70%	13.00%
Btg2	1.04	3.4E-10	22.80%	13.30%
Errfi1	1.20	6.0E-21	41.50%	20.60%
Nr4a1	1.33	3.7E-21	35.00%	13.30%
D. Genes differentially expressed between SCARKO and WT in interstitial progenitor				
Gene	**FC(log2)**	***P* val**	**%SCARKO**	**%WT**
Acta2	–1.81	9.7E-14	8.10%	15.10%
Tpm2	–1.16	1.3E-12	17.40%	23.00%
Crip1	–1.06	7.8E-13	17.20%	24.00%
E. Genes differentially expressed between SCARKO and WT in macrophages				
Gene	**FC(log2)**	***P* val**	**%SCARKO**	**%WT**
Gm13680	–1.24	4.6E-11	9.90%	19.80%
Cst9	–1.16	1.2E-20	16.80%	18.50%
Gm13456	–1.15	5.3E-08	11.20%	19.90%
Cst12	–1.12	9.7E-21	19.50%	22.10%
Gm6136	–1.04	3.1E-11	16.10%	27.40%
Sept11	–1.03	1.2E-07	10.90%	17.10%
Rps27a-ps2	–1.00	1.2E-08	14.90%	23.00%
Tgfb1	0.95	1.5E-06	17.50%	9.70%
Apoc1	1.02	5.8E-11	23.80%	9.00%

Gene filter criteria: > 2-fold change in either direction and detection rate > 15% in either WT or SCARKO. A negative FC value means lower expression in SCARKO. FC is in log(base = 2) scale.

TABLE 2: Genes differentially expressed between SCARKO and WT in five somatic cell types. Continued

number in the juvenile testis (O'Shaughnessy *et al.*, 2002), the earlier report relied on Cyp11A1 staining to quantify Leydig cell number, but Cyp11A1 cannot distinguish between immature and mature Leydig cells. Therefore the shift in immature/mature Leydig numbers we observe would not be evident by Cyp11A1 immunostaining. However, the O'Shaughnessy *et al.* (2002) study found that Leydig cell numbers drop in the aging testis, suggesting that alterations of population dynamics in extratubular somatic populations become more pronounce after subsequent rounds of spermatogenesis and onset of puberty.

Sertoli-cell androgen signaling is required for the normal germ-cell transcriptome and for onset of meiotic divisions

Male germ cells lack cell-autonomous AR expression, yet a large body of evidence demonstrates that androgen signaling from surrounding Sertoli cells is required for normal progress through spermatogenesis (O'Hara and Smith, 2015). In addition to the known spermatocyte meiotic arrest in SCARKO testes, we show here that germ cells undergo pervasive apoptosis throughout meiotic prophase. These data show that androgen signaling from Sertoli cells throughout meiotic prophase is critical, most probably by providing a nurturing environment for germ cells. Importantly, however, a subset of spermatocytes survive and progress normally through central meiotic processes, undergoing chromosome pairing and synapsis, XY body formation, and and expressing markers of meiotic recombination (Figure 3). Hence, quintessential prophase chromosomal dynamics, defining events from leptotene to midpachytene, can occur independently of androgen signaling from Sertoli cells. However, despite an apparently normal chromosomal progression, SCARKO spermatocytes are not competent to undergo the natural transition from meiotic prophase to the division phase, nor are they competent to respond to a pharmacological agent that promotes premature transition from meiotic prophase (Figure 3H). Together, the phenotype of normal cytological features of

mid pachynema combined with lack of competence to progress to the division phase suggests that androgen signaling is required for germ cells to acquire competence for meiotic division and subsequent spermiogenesis.

Very little is known about spermatocyte gene expression required for meiotic division-phase competence, an issue directly tackled by this study. At a general level, it is known that gene expression changes during meiotic prophase are extensive (De Gendt *et al.*, 2014; Chen *et al.*, 2018; Green *et al.*, 2018; Jung *et al.*, 2019), with modules or clusters of genes expressed at appropriate times for ongoing prophase events (Jung *et al.*, 2019). Nonetheless, genes known to be required for fertility tend to reach peak expression levels in a cell stage at or preceding the stage of observed cytological arrest (Green *et al.*, 2018). Moreover, bulk tissue sample analysis also reveal that some transcripts are expressed in prophase spermatocytes but are not required or translated until postmeiotic spermiogenesis (Ball *et al.*, 2016). Our goal here was to define the androgen-dependent molecular signature and the precise germ cell stage of arrest. Our cytological and scRNAseq analyses showed that the majority of SCARKO germ cells experienced a transcriptomic stall point at the leptotene/zygotene transition, but progressed further based on cytological assessment. The transcriptomic arrest of most SCARKO spermatocytes at a leptotene-zygotene state raised the question not only of function of genes failing to be expressed but also whether there might be aberrant gene expression at even earlier stages of spermatogenesis. In fact, some of the genes identified as differentially expressed in the leptotene/zygotene mutant transcriptomes were expressed earlier (Table 1), as early as in GC2 (*Ldhc, Meig1*, and *Fabp9*). The remaining misregulated genes were specifically expressed in leptotene/zygotene (*Crisp2, Meig1, Spink2*, and *Gstm5*; Table 1). Some of the identified genes are required for organization of the cytoskeleton, acrosome, or cilia, structures that are formed in later germ cells; therefore, it appears that transcripts required for meiotic and spermiogenic competence are accumulated prior to the time of their developmental need.

In the absence of a functional Sertoli-cell AR, germ cells progressively acquire aberrant transcriptomic attributes (a germ-cell "SCARKO molecular phenotype"), culminating in a terminal leptotene-zygotene transcriptional signature with failure to progress to subsequent transcriptomic signatures. In spite of this pervasive transcriptomic block, a few (~4% of the sequenced germ cells) mutant spermatocytes are found in the early–midpachytene cluster. The small subset of cells that escape the leptotene/zygotene transcriptional block may correspond to the rare spermatocytes in the SCARKO testes that are capable of condensing chromosomes in response to OA treatment in vitro (Figure 3, G and H).

Our findings highlights a discrepancy between a seemingly normal meiotic progress of surviving spermatocytes to the midpachytene stage, as observed with cytology analysis, and an apparent transcriptional arrest for most cells at an earlier stage (comparable to the WT transcriptome of leptotene-zygotene spermatocytes). Thus it should not be assumed that cytological and/or morphological states are necessarily coupled with corresponding molecular transcriptomic states. Indeed, a similar transcriptional uncoupling effect was recently found by studying a *Prdm9* mutation (Fine *et al.*, 2019), a gene required for selective activation of hotspots of meiotic recombination. In this report, *Prdm9* mutant germ cells exhibited cytological arrest at a prepachytene stage, but RNA-seq analyses revealed expression of genes that are normally activated later in meiotic prophase that support subsequent spermiogenesis. Together, these findings suggest that the temporal pace of gene activation and expression is not necessarily tied to the temporal events of meiotic prophase chromosomal dynamics.

In conclusion, synchronization of spermatogenesis coupled with scRNAseq analysis of SCARKO and aged-matched WT testes enabled us to identify and molecularly dissect the precise time point of androgen-dependent germ-cell arrest. Our observations suggest that the Sertoli cells themselves create a permissive environment for meiosis and subsequent spermiogenesis. Future studies stand to discover unknown mechanisms underlying critical meiotic prophase transitions in spermatogenisis by investigating the specific genes identified here.

MATERIALS AND METHODS

Animals

All experiments were conducted following Institutional Animal Care and Use Committee (IACUC) at The Jackson Laboratory and University of Michigan. All mice used in our experiments were obtained from a mixed genetic background C57BL/6; 129/SvEv. Specifically, we crossed the *Ar* $^{fl/fl}$ females (Chakraborty *et al.*, 2014) with Amh-cre $^{tg/+}$ (Lécureuil *et al.*, 2002), yielding ~50% of the resulting males lacking AR in Sertoli cells (hereafter referred to as SCARKO). The Amh-Cre^{-} male littermates were used as WT controls. Animal genotypes were confirmed by PCR as previously described (Chang *et al.*, 2004).

Synchronization of seminiferous epithelium

Onset of spermatogenesis was synchronized as previously described (Hogarth *et al.*, 2013). Briefly, WIN 18,446 was administered to pups orally from 2 to 8 dpp at a dose of approximately 100 mg/kg/d. At 9 dpp, pups were given an IP injection of RA (100 μg/animal). Testes were collected between 6 and 16 d following the RA injection (Table 1).

Meiotic chromosome spreads

Meiotic spreads were prepared as previously described (Peters *et al.*, 1997). Briefly, testes were harvested, detunicated, and then incubated for 45 min in hypotonic-extraction buffer (30 mM Tris-HCl, 50 mM sucrose, 17 mM sodium citrate, 5 mM EDTA, 2.5 mM dithiothreitol, 0.5 mM phenylmethylsulfonyl fluoride, and 1× protease inhibitor). Cells were mixed in 100 mM sucrose and spread on slides that were prewashed with 0.5% PFA/0.05% Triton X-100. Slides were kept in a humid chamber for approximately 16 h at 4°C. Slides were then air dried, washed in 0.04% Photo-Flo 200 solution (Electron Microscopy Sciences) in ddH2O for 1 h, and air-dried completely. The slides were then either stained immediately or stored at –20°C for later use.

Immunofluorescence

For immunostaining chromosome spreads, slides were blocked for 1 h at room temperature in blocking buffer (0.3% bovine serum albumin [BSA], 1% goat serum in phosphate-buffered saline [PBS] with 0.05% Triton X-100). The slides were incubated with primary antibodies approximately 16 h at 4°C. Immunolabeling was done using the following primary antibodies: guinea pig anti-H1t (1:100, Handel Laboratory), mouse anti-γH2AX (1:100, Invitrogen Cat# MA1-2022), mouse anti-MLH1 (1:20, Abcam Cat# ab14206), rabbit anti-SYCP1 (1:100, Novus Biologicals Cat# nb300-229), rabbit anti-SYCP3 (1:100, Novus Biologicals Cat# nb300-232), and rat anti-SYCP3 (1:100, Handel Laboratory). Slides were washed with the blocking buffer and incubated for 4 h with conjugated secondary antibodies and counterstained with DAPI to identify nuclei. Secondary antibodies conjugated with either Alexa 488 or Alexa 594 were

used for these analyses (Thermo Fisher Scientific). Cells were visualized and quantified using a microscope (Leica Leitz DMRD).

TUNEL staining

Testes were collected, fixed in 4% PFA (in PBS) for approximately 16 h at 4°C, dehydrated in ethanol wash series, and embedded in paraffin. Four-micron formalin fixed paraffin embedded (FFPE) tissue sections were deparaffinized, rehydrated, and boiled in 0.01 M sodium citrate, pH 6.0, for 3 min. After antigen retrieval, tissue sections were blocked in 20% horse serum, 0.3% BSA in PBS for 30 min at room temperature, and processed following the Roche Applied TUNEL kit. All images collected used a Leica Leitz DMRD microscope. The percentage of TUNEL-positive cells was determined by averaging at least 100 tubules for each sample.

In vitro induction of metaphase

This procedure was adapted from several sources (Evans *et al*., 1964; Wiltshire *et al*., 1995; Cobb *et al*., 1999). Briefly, testes were dissociated using 0.5 mg/ml collagenase-diluted DMEM + 25 mM HEPES for 20 min at 37°C with shaking, washed 3× in DMEM, and then digested with 0.5 mg/ml trypsin for 12 min at 37°C with shaking to generate a single-cell suspension. The mixed-germ cell suspension were filtered through a 70-micron Nitex mesh and washed 3× in DMEM + 25 mM HEPES medium. Approximately 100,000 cells were placed into culture dish and treated with either 400 µM OA stock solution or vehicle (100% ethanol), respectively, for 4 h. The cultured spermatocytes were collected through centrifugation and washed in 2.2% sodium citrate, then 1% sodium citrate. The cells were then fixed (3:1 ratio of 100% ethanol; glacial acetic acid with 2% chloroform) for 5 min at room temperature with gentle rocking. Fixed germ cells were then dropped from a height of approximately 0.5 m on a glass slide and were allowed to air-dry before being stained with Giemsa for the presence of condensed metaphase cells.

Isolation of single cells for sequencing

Testes from transgenic SCARKO mice and WT litter mates were transferred to 10 ml of digestion buffer 1 (comprised of Advanced DMEM:F12 media [ThermoFisher Scientific], 200 mg/ml Collagenase IV [Sigma], and 400 U/ml DNase I [Sigma]). Tubules were dispersed by gently shaking by hand and allowed to settle for 1 min at room temperature. The supernatant was collected, placed on ice and quenched with the addition of fetal bovine serum (FBS) (Thermo Fisher Scientific). The remaining tubules were then transferred to digestion buffer 2 (0.25 mg/ml trypsin [ThermoFisher Scientific] and 400 U/ml DNase I [Sigma] dissolved in Advanced DMEM:F12 media) and dissociated at 35°C/215 rpm for 5 min each. Any remaining tubule fragments were broken up with manual agitation using a 1000-µl pipette. The resulting single cell suspension was transferred to the previously collected supernatant and quenched with the addition of FBS (Thermo Fisher Scientific). Cells were filtered through a 100-µm strainer, washed in PBS, pelleted at 300 × *g* for 5 min, and resuspended in MACS buffer containing 0.5% BSA (Miltenyi Biotec). For all Drop-seq experiments, the live single-cell suspensions were collected by flow cytometry using (FACS) ARIA II/III (BD Biosciences) cell sorter.

Drop-seq procedure

Single-cell suspensions were diluted to 250 cells/microliter and processed as described previously (Macosko *et al*., 2015; Green *et al*., 2018). Briefly, cells, barcoded microparticle beads (MACOSKO-2011-1-0, Lots 072817 and 060718, ChemGenes Corporation), and lysis buffer were coflown into a microfluidic device and captured in nanoliter-sized droplets. After droplet collection and breakage, the beads were washed, and cDNA synthesis occurred on the bead using Maxima H-minus RT (Thermo Fisher Scientific) and the Template Switch Oligo. Excess oligos were removed by exonuclease I digestion (New England Biosciences). cDNA amplification was done for 15 cycles from pools of 2000 beads using HotStart ReadyMix (Kapa Biosystems) and the SMART PCR primer. Individual PCRs were purified and pooled for library generation. A total of 600 pg of amplified cDNA was used for a Nextera XT library preparation (Illumina) with the New-P5-SMART PCR hybrid oligo and a modified P7 Nextera oligo with 10-base pair barcodes. Sequencing was performed on a HiSeq-4000 (Illumina) 26 × 115 base pair paired end sequening using Read1CustomSeqB primer.

Template Switch Oligo	Drop-seq RT	AAGCAGTGGTATCAACGCAGAGTGAATrGrGrG
SMART PCR primer	Drop-seq PCR	AAGCAGTGGTATCAACGCAGAGT
New-P5-SMART PCR hybrid oligo	Drop-seq library PCR	AATGATACGGCGACCACCGAGATCTACACGCCTGTCCGCG-GAAGCAGTGGTATCAACGCAGAGT*A*C
Custom P7 index oligo 0	Drop-seq library PCR	CAAGCAGAAGACGGCATACGAGATTCGGCTTGCGGTCTC-GTGGGCTCGG
Custom P7 index oligo 1	Drop-seq library PCR	CAAGCAGAAGACGGCATACGAGATTGACTCGCAAGTCTC-GTGGGCTCGG
Custom P7 index oligo 4	Drop-seq library PCR	CAAGCAGAAGACGGCATACGAGATTGGAAGCAATGTCTC-GTGGGCTCGG
Custom P7 index oligo 6	Drop-seq library PCR	CAAGCAGAAGACGGCATACGAGATAGCGTAACTCGTCTC-GTGGGCTCGG
Custom P7 index oligo 8	Drop-seq library PCR	CAAGCAGAAGACGGCATACGAGATGAACGATAAAGTCTC-GTGGGCTCGG
Custom P7 index oligo 10	Drop-seq library PCR	CAAGCAGAAGACGGCATACGAGATCAGTATCCGGGTCTC-GTGGGCTCGG
Read1CustomSeqB	Drop-seq sequencing	GCCTGTCCGCGGAAGCAGTGGTATCAACGCAGAGTAC

Computational analysis of Drop-seq data

Data processing, quality filtering, and normalization. We analyzed eight samples corresponding to mouse testes from two genetic lines: WT and SCARKO mutant, collected at four time points: 8, 13, and 16 dpi and 21 dpp. The paired-end Drop-seq data for the eight samples were sequenced in two runs (8 and 13 dpi in one, 16 dpi and 21 dpp in the other) and were processed using *Drop-seq tools* v1.13 from the McCarroll laboratory as described before (Macosko *et al.*, 2015; Shekhar *et al.*, 2016). Specifically, the reads were aligned to the mouse reference genome (GRCm38, version 38) using *STAR* v2.5.2b (Dobin *et al.*, 2013). The pipeline generated digital gene expression matrices with genes as rows and cells as columns that served as the starting point for downstream analyses.

We filtered cells by quality measures related to the depth of sequencing and estimated cell integrity. Cells with < 500 detected genes or with > 10% of transcripts corresponding to mitochondria-encoded genes were removed, as previously described (Green *et al.*, 2018). This left us with 1688–4038 post-QC cells in each of the eight datasets, for a total of 21,314 cells. Among these cells the average number of UMIs was 4043, and the average number of detected genes per cell was 1809.

We generated the normalized data for each cell by 1) dividing the UMI counts by the total number of UMIs of that cell and 2) multiplying by 10,000 to obtain a transcripts-per-10,000 measure and 3) log-transforming it by E = ln(transcripts-per-10,000 + 1). For some downstream analyses, we also standardized for each gene: its expression levels across cells are transformed by using (E-mean(E))/sd(E).

Batch correction and clustering to identify major cell types. Pass-QC cells from all eight samples were combined and batch-corrected by aligning similar cell profiles across samples using the canonical correlation analysis (CCA) method in the R package *Seurat* v2.3.4 (Hardoon *et al.*, 2004; Butler *et al.*, 2018). The CCA analysis was based on 1) selecting the top 2000 highly variable genes from each dataset using the standard procedure in *Seurat* and 2) merging the gene lists to obtain the union of highly variable genes. The top three aligned CCs—as determined by the MetageneBicorPlot—were used for Louvain-Jaccard clustering of the cells, resulting in seven clusters (Figure 4A) at a resolution of 0.3. We performed tSNE using the top aligned CCs to project the cells at reduced dimensions. The relative contribution of the eight samples to the seven cell types was shown in tSNE plots (Supplemental Figure S1B). The seven clusters were annotated to known cell types both by the expression patterns of known genes (examples shown in Supplemental Figure S2) and by systematically evaluating markers identified computationally for each cluster. This is done by comparing cells in this cluster with those in the other seven clusters and selecting markers using three criteria of differential expression (DE): 1) at least 20% higher fraction-of-detection in the cluster compared with all other clusters, 2) at least twofold higher average expression in the cluster, and 3) a binomial test p value, after multiple-testing correction, is < 0.01. The markers thus obtained are shown in Figure 4C and Supplemental Table S2.

Evaluating reproducibility of identified cell types across batches. While CCA analysis described above allowed us to use top CCs for tSNE projection and Louvain-Jaccard clustering (e.g., Figures 4A and 6A), *Seurat* does not provide a transparent way to export CC-corrected gene expression values. Further, WT and SCARKO samples have genuine biological differences in the number of cells belonging to different cell types and cannot be simply considered as samples with only technical differences. To obtain postcorrection data for downstream analyses, we systematically evaluated the centroid-to-centroid "distances" both across the seven cell types and across the eight samples. This exploration revealed that the WT samples at the two later time points (16 dpi and 21 dpp) had systematic shifts from the other six samples and the shifts were parallel for the seven cell types (not shown), indicating a batch effect shared by all cells. We recentered gene expression levels for the two empirically defined batches—WT16dpi and WT21dpp in one and the rest in another—to obtain postcorrection data. Batch centroid is obtained by averaging the normalized expression level, on the linear scale, for all cells within the batch, then taking the log: ln(mean of normalized expression+1). We then compared the seven postcorrection cluster centroids among the eight samples by cross-tabulated rank correlation coefficients, calculated using 2K HVG, among all pairs of cluster centroids across the eight samples (Supplemental Figure S1A), which demonstrated that identified cell types were consistently observed across batches.

Focused reclustering analyses for germ cell. We extracted the germ cells from all eight samples (spermatogonia and spermatocytes, N = 3185, with 2385 WT and 800 SCARKO cells), selected HVG and standardized for genes for germ cells, and performed PCA using HVG. To reassess cellular heterogeneity just for the germ cells, we performed Louvain-Jaccard clustering to identify cell clusters using the top eight PCs (Blondel *et al.*, 2008). This identified seven clusters corresponding to seven consecutive germ cell states, termed GC1 to GC7, as shown in Figure 5A. We repeated the same marker identification steps following the selection criteria described above (Figure 5B). To compare the shifts of germ cell states across the eight samples, we collapse the seven states to four and calculated the proportion of cells over the four states for each samples (Figure 5C).

DE analysis in germ cells. We performed two types of DE analysis. First, to identify genes dynamically regulated over the course of germ cell development, we identified marker genes for each GC by comparing it with the other six GC states (combining the genotypes and time points) using the binomial likelihood test embedded in *Seurat* with a minimum of twofold change and $p < 0.01$ (Supplemental Table S3). Second, to identify genes differentially expressed between SCARKO and WT within GC2, GC3, or GC4, we performed DE analysis using the same parameters as above, using cells within each state (Figure 5D). Top genes are provided in Table 1, which also included results of pathway analysis using *LRPath (*Kim *et al.*, 2012).

Focused reclustering analyses for somatic cell. From the global analysis of all cells we defined seven clusters, including five somatic cell type clusters. We extracted somatic cells with an additional filter to remove suspected doublets (N = 95). Somatic cells (N = 18,203) from all eight samples were merged and batch-corrected by CCA using 2000 HVG selected specific for somatic cells. We performed Louvain-Jaccard clustering using top eight aligned CCs, resulting in five somatic cell types. The five somatic cell types thus identified (Figure 6, A and B) had high concordance (not shown) with the somatic cell clusters in the global analysis (previously Figure 4A), which included both germ cells and somatic cells. The relative proportion of the five somatic cell types was compared across genotypes and time points (Figure 6C).

Sertoli cell analysis. We extracted 1198 Sertoli cells, selected ~4000 HVG, and standardized each gene across Sertoli cells. We performed PCA using HVG for Sertoli cells and did focused reprojection in t-SNE space using top 4 PCs (Figure 6D). DE analysis between WT and SCARKO was done as before—using the binomial likelihood test with a minimum of 1.5-fold-change and $p < 0.01$. The results are presented in Figure 6E and Table 2.

Genomics data

All genomics data are deposited in GEO under the accession GSE151564. All codes used for figure generation are provided in gitHub; see https://github.com/qianqianshao/SCARKO.

ACKNOWLEDGMENTS

We thank members of the Hammoud, Li, and Handel labs for scientific discussions and manuscript comments. We acknowledge the able assistance of Catherine Brunton for maintenance of mice and Karen Davis for assistance in preparing figures. This research was supported by National Institutes of Health (NIH) grants HD33816 (M.A.H.), 1R21HD090371-01A1 (S.S.H. and and J.Z.L.), 1DP2HD091949-01 (S.S.H.), and F30HD097961 (A.N.S); Michigan Institute for Data Science (MIDAS) grant for Health Sciences Challenge Award (J.Z.L. and S.S.H.); CTRB training grant 5T32HD079342-04 (A.N.S.); MSTP training grant 5T32GM007863-38 (A.N.S.); Open Philanthropy Grant 2019-199327 (5384, S.S.H.); and partially supported by NIH P30 CA034196 to the Jackson Laboratory. The content is solely the responsibility of the authors and does not necessarily represent the official views of the NIH.

REFERENCES

Anguera MC, Ma W, Clift D, Namekawa S, Kelleher RJ, Lee JT (2011). Tsx produces a long noncoding RNA and has general functions in the germline, stem cells, and brain. PLoS Genet 7, e1002248.

Ball RL, Fujiwara Y, Sun F, Hu J, Hibbs MA, Handel MA, Carter GW (2016). Regulatory complexity revealed by integrated cytological and RNA-seq analyses of meiotic substages in mouse spermatocytes. BMC Genomics 17, 628.

Bi J, Li Y, Sun F, Saalbach A, Klein C, Miller DJ, Hess R, Nowak RA (2013). Basigin null mutant male mice are sterile and exhibit impaired interactions between germ cells and Sertoli cells. Dev Biol 380, 145–156.

Blondel VD, Guillaume J-L, Lambiotte R, Lefebvre E (2008). Fast unfolding of communities in large networks. J Stat Mech 2008, P10008.

Bolcun-Filas E, Handel MA (2018). Meiosis: the chromosomal foundation of reproduction. Biol Reprod 99, 112–126.

Butler A, Hoffman P, Smibert P, Papalexi E, Satija R (2018) Integrating single-cell transcriptomic data across different conditions, technologies, and species. Nat Biotechnol 36, 411–20.

Chakraborty P, William Buaas F, Sharma M, Smith BE, Greenlee AR, Eacker SM, Braun RE (2014). Androgen-dependent Sertoli cell tight junction remodeling is mediated by multiple tight junction components. Mol Endocrinol 28, 1055–1072.

Chang C, Chen Y-T, Yeh S-D, Xu Q, Wang R-S, Guillou F, Lardy H, Yeh S (2004). Infertility with defective spermatogenesis and hypotestosteronemia in male mice lacking the androgen receptor in Sertoli cells. Proc Natl Acad Sci USA 101, 6876–6881.

Chen S-R, Hao X-X, Zhang Y, Deng S-L, Wang Z-P, Wang Y-Q, Wang X-X, Liu Y-X (2016). Androgen receptor in Sertoli cells regulates DNA double-strand break repair and chromosomal synapsis of spermatocytes partially through intercellular EGF-EGFR signaling. Oncotarget 7, 18722–18735.

Chen Y, Zheng Y, Gao Y, Lin Z, Yang S, Wang T, Wang Q, Xie N, Hua R, Liu M, *et al*. (2018). Single-cell RNA-seq uncovers dynamic processes and critical regulators in mouse spermatogenesis. Cell Res 28, 879–896.

Cobb J, Cargile B, Handel MA (1999). Acquisition of competence to condense metaphase I chromosomes during spermatogenesis. Dev Biol 205, 49–64.

De Gendt K, Swinnen JV, Saunders PT, Schoonjans L, Dewerchin M, Devos A, Tan K, Atanassova N, Claessens F, Lecureuil C, *et al*. (2004). A Sertoli cell-selective knockout of the androgen receptor causes spermatogenic arrest in meiosis. Proc Natl Acad Sci USA 101, 1327–1332.

De Gendt K, Verhoeven G, Amieux PS, Wilkinson MF (2014). Genome-wide identification of AR-regulated genes translated in Sertoli cells in vivo using the RiboTag approach. Mol Endocrinol 28, 575–591.

Dobin A, Davis CA, Schlesinger F, Drenkow J, Zaleski C, Jha S, Batut P, Chaisson M, Gingeras TR (2013). STAR: ultrafast universal RNA-seq aligner. Bioinformatics 29, 15–21.

Evans EP, Breckon G, Ford CE (1964). An air-drying method for meiotic preparations from mammalian testes. Cytogenetics 3, 289–294.

Fine AD, Ball RL, Fujiwara Y, Handel MA, Carter GW (2019). Uncoupling of transcriptomic and cytological differentiation in mouse spermatocytes with impaired meiosis. Mol Biol Cell 30, 717–728.

Green CD, *et al*. (2018). A comprehensive roadmap of murine spermatogenesis defined by single-cell RNA-Seq. Dev Cell 46, 651–667.e10.

Griswold MD (2016). Spermatogenesis: the commitment to meiosis. Physiol Rev 96, 1–17.

Hardoon DR, Szedmak S, Shawe-Taylor J (2004) Canonical correlation analysis: an overview with application to learning methods. Neural Comput 16, 2639–64.

Hogarth CA, Arnold S, Kent T, Mitchell D, Isoherranen N, Griswold MD (2015). Processive pulses of retinoic acid propel asynchronous and continuous murine sperm production. Biol Reprod 92, 37.

Hogarth CA, Evanoff R, Mitchell D, Kent T, Small C, Amory JK, Griswold MD (2013). Turning a spermatogenic wave into a tsunami: synchronizing murine spermatogenesis using WIN 18,446. Biol Reprod 88, 40.

Inselman A, Eaker S, Handel MA (2003). Temporal expression of cell cycle-related proteins during spermatogenesis: establishing a timeline for onset of the meiotic divisions. Cytogenet Genome Res 103, 277–284.

Johnston DS, Russell LD, Friel PJ, Griswold MD (2001). Murine germ cells do not require functional androgen receptors to complete spermatogenesis following spermatogonial stem cell transplantation. Endocrinology 142, 2405–2408.

Jordan PW, Karppinen J, Handel MA (2012). Polo-like kinase is required for synaptonemal complex disassembly and phosphorylation in mouse spermatocytes. J Cell Sci 125, 5061–5072.

Jung M, Wells D, Rusch J, Ahmad S, Marchini J, Myers SR, Conrad DF (2019). Unified single-cell analysis of testis gene regulation and pathology in five mouse strains. Elife 8.

Kent T, Bhattacharyya T, and Handel MA (2019). Genetic analysis of meiotic chromosome dynamics and fertility. In: Human Reproductive and Prenatal Genetics, ed. PKC Leung and J Qiao, New York: Academic Press.

Kim JH, Karnovsky A, Mahavisno V, Weymouth T, Pande M, Dolinoy DC, Rozek LS, Sartor MA (2012) LRpath analysis reveals common pathways dysregulated via DNA methylation across cancer types. BMC Genomics 13, 526.

Kott E, *et al*. (2013). Loss-of-function mutations in RSPH1 cause primary ciliary dyskinesia with central-complex and radial-spoke defects. Am J Hum Genet 93, 561–570.

Lécureuil C, Fontaine I, Crepieux P, Guillou F (2002). Sertoli and granulosa cell-specific Cre recombinase activity in transgenic mice. Genesis 33, 114–118.

Lin Q, Sirotkin A, Skoultchi AI (2000). Normal spermatogenesis in mice lacking the testis-specific linker histone H1t. Mol Cell Biol 20, 2122–2128.

Lindsey JS, Wilkinson MF (1996). An androgen-regulated homeobox gene expressed in rat testis and epididymis. Biol Reprod 55, 975–983.

Macosko EZ. *et al*. (2015). Highly parallel genome-wide expression profiling of individual cells using nanoliter droplets. Cell 161, 1202–1214.

O'Hara L, Smith LB (2015). Androgen receptor roles in spermatogenesis and infertility. Best Pract Res Clin Endocrinol Metab 29, 595–605.

O'Shaughnessy PJ, Johnston H, Willerton L, Baker PJ (2002). Failure of normal adult Leydig cell development in androgen-receptor-deficient mice. J Cell Sci 115, 3491–3496.

Peters AHFM, Plug AW, de Boer P (1997). Meiosis in carriers of heteromorphic bivalents: sex differences and implications for male fertility. Chromosome Res 5, 313–324.

Shekhar K, Lapan SW, Whitney IE, Tran NM, Macosko EZ, Kowalczyk M, Adiconis X, Levin JZ, Nemesh J, Goldman M, *et al*. (2016). Comprehensive classification of retinal bipolar neurons by single-cell transcriptomics. Cell 166, 1308–1323.e1330.

Snyder E, Soundararajan R, Sharma M, Dearth A, Smith B, Braun RE (2015). Compound heterozygosity for Y box proteins causes sterility due to loss of translational repression. PLoS Genet 11, e1005690.

Sun F, Handel MA (2008). Regulation of the meiotic prophase I to metaphase I transition in mouse spermatocytes. Chromosoma 117, 471–485.

Tan KA, Turner KJ, Saunders PT, Verhoeven G, De Gendt K, Atanassova N, Sharpe RM (2005). Androgen regulation of stage-dependent cyclin D2 expression in Sertoli cells suggests a role in modulating androgen action on spermatogenesis. Biol Reprod 72, 1151–1160.

Uhrin P, *et al*. (2000). Disruption of the protein C inhibitor gene results in impaired spermatogenesis and male infertility. J Clin Invest 106, 1531–1539.

Willems A, De Gendt K, Allemeersch J, Smith LB, Welsh M, Swinnen JV, Verhoeven G (2010). Early effects of Sertoli cell-selective androgen receptor ablation on testicular gene expression. Int J Androl 33, 507–517.

Wiltshire T, Park C, Caldwell KA, Handel MA (1995). Induced premature G2/M-phase transition in pachytene spermatocytes includes events unique to meiosis. Dev Biol 169, 557–567.

Zhang F-P, *et al*. (2019). Lack of androgen receptor SUMOylation results in male infertility due to epididymal dysfunction. Nat Commun 10, 777.

Zhou W, Wang G, Small CL, Liu Z, Weng CC, Yang L, Griswold MD, Meistrich ML (2010). Gene expression alterations by conditional knockout of androgen receptor in adult Sertoli cells of. Biol Reprod 83, 759–766.